Climate Projection of Tropical Cyclone Lifetime in the Western North Pacific Basin

THE-ANH VU,[a] CHANH KIEU,[a] SCOTT M. ROBESON,[b] PAUL STATEN,[a] AND BEN KRAVITZ[a,c]

[a] *Department of Earth and Atmospheric Sciences, Indiana University Bloomington, Bloomington, Indiana*
[b] *Department of Geography, Indiana University Bloomington, Bloomington, Indiana*
[c] *Atmospheric Sciences and Global Change Division, Pacific Northwest National Laboratory, Richland, Washington*

(Manuscript received 24 February 2024, in final form 17 October 2024, accepted 22 October 2024)

ABSTRACT: In this study, the potential changes in tropical cyclone (TC) lifetime in the western North Pacific basin are examined for different future climates. Using homogeneous 9-km-resolution dynamical downscaling with the Weather Research and Forecasting (WRF) Model, we show that TC-averaged lifetime displays insignificant change under both low and high greenhouse gas concentration scenarios. However, more noticeable changes in the tails of TC lifetime statistics are captured in our downscaling simulations, with more frequent long-lived TCs (lifetime of 8–11 days) and less short-lived TCs (lifetime of 3–5 days). Unlike present-day simulations, it is found that the correlation between TC lifetime and the Niño index is relatively weak and insignificant in all future downscaling simulations, thus offering little explanation for these changes in TC lifetime statistics based on El Niño–Southern Oscillation. More detailed analyses of TC track distribution in the western North Pacific basin reveal, nevertheless, a noticeable shift of TC track patterns toward the end of the twenty-first century. Such a change in TC track climatology results in an overall longer duration of TCs over the open ocean, which is consistent across future scenarios and periods examined in this study. This shift in the TC track pattern is ultimately linked to changes in the western North Pacific subtropical high, which retreats to the south during July and to the east during August–September. The results obtained in this study provide new insights into how large-scale circulations can affect TC lifetime in the western North Pacific basin in warmer climates.

SIGNIFICANCE STATEMENT: Using high-resolution dynamical downscaling with the Weather Research and Forecasting (WRF) Model under low- and high-emission scenarios, this study shows that the basin-averaged tropical cyclone (TC) lifetime in the western North Pacific (WNP) basin has no noticeable change under both warmer climate scenarios, despite an overall increase in TC maximum intensity. However, the tails of the TC lifetime distribution display significant changes, with more long-lived (6–20 days) TCs but less short-lived (3–5 days) TCs in the future. These changes in TC lifetime statistics are caused by the shift of the North Pacific subtropical high, which alters large-scale steering flows and TC track patterns. These results help explain why previous studies on TC lifetime projections have been inconclusive in the WNP basin and provide new insights into how large-scale circulations can modulate TC lifetime in a warmer climate.

KEYWORDS: Hurricanes/typhoons; Climate variability; Interdecadal variability; Trends; Tropical variability

1. Introduction

Improving the projection of tropical cyclone (TC) activities under different climate scenarios is essential for better future risk management and preparation. Any such improved TC projection is of great importance in the western North Pacific (WNP) basin where the impacts of TCs are known to be extensive for countries with long coastlines (Kossin et al. 2016; Peduzzi et al. 2012; Tran-Quang et al. 2020; Trinh et al. 2021). This WNP basin (0°–40°N, 100°E–180°) is statistically one of the most active regions in TC climatology, which accounts for one-third of global TCs with an average of 25–30 TCs every year (Lee et al. 2019; Defforge and Merlis 2017; Thanh et al. 2020).

From a broader perspective, all main characteristics of TCs—such as frequency, intensity, accumulated rainfall, or track distribution—are strongly modulated by climate variability (e.g., Chan 2008). Numerous modeling studies using sea surface temperature (SST) forcings under different Intergovernmental Panel on Climate Change (IPCC) climate scenarios have captured noticeable changes in these TC characteristics, especially frequency and intensity statistics (e.g., Knutson et al. 1998; Oouchi et al. 2006; Walsh et al. 2007; Bengtsson et al. 2007; T.-C. Lee et al. 2020; Cha et al. 2020; Camargo et al. 2023). For example, an early modeling study by Knutson et al. (1998) showed that TCs in the WNP tend to be stronger by 3–7 m s^{-1} under the doubled-carbon dioxide (CO_2) warming scenario as compared to the present-day (PD) climatology.

Using higher-resolution global atmospheric models, Oouchi et al. (2006) demonstrated further that the geographical distribution of TCs would likely remain unchanged, but TC frequency appeared to decrease noticeably in a warmer climate—a result supported by many later studies (e.g., Sugi et al. 2002; McDonald et al. 2005; Oouchi et al. 2006; Zhao et al. 2009; Kieu et al. 2023). Although there is no extant theory for the decrease in TC frequency in a warmer climate, the increase in TC intensity in a warmer climate is consistent with current theoretical analyses such as the maximum potential intensity frameworks

Corresponding author: Chanh Kieu, ckieu@iu.edu

DOI: 10.1175/JCLI-D-24-0131.1

by, e.g., Emanuel (1987) or Holland (1997). Specifically, these theories for TC intensity all suggest an increasing trend of TC potential intensity in a warmer SST environment.

Among many aspects of TC activities that have been extensively studied, TC lifetime in the WNP basin has received less attention so far due likely to the confounding effects of multiple large-scale systems that govern TC lifetime. Several studies have attempted to quantify TC lifetime variability in future climates, but their findings remain inconclusive and somewhat inconsistent at present. For example, a study by Murakami et al. (2011) suggested that TC lifetime tends to increase due to the eastward shift of TC tracks, yet this lifetime increase could not be reliably quantified. According to their study, such an eastward TC displacement was caused by the retreat of the western Pacific subtropical high (WPSH), leading to the weakening of the easterly flow. As a result, TCs are redirected to a warm open ocean area in the far-east WNP, decreasing their likelihood of landfall and extending their lifetime (Chan and Liu 2004; Murakami et al. 2011). Similar to Murakami et al. (2011), Lee et al. (2019) found that future TCs have a longer lifetime (+6.6%) and a stronger intensity (+4.1%).

In their experiments with 16-km-resolution global atmospheric general circulation models, Manganello et al. (2014) found, however, that the overall lifetime distribution of TC future simulation did not change significantly. Their estimation gave a range from +0.02 to 0.06 day difference in TC lifetime between the future and the PD climate simulations, despite a southward shift of TCs due to the stronger monsoon trough and a southward extension of the WPSH. In contrast, the study by Hong et al. (2021) showed that TC lifetime in a warmer climate would be shortened by a half day due to a poleward shift of TC genesis and faster TC propagation in the WNP. The reason for such shortened TC lifetime in Hong et al. (2021)'s study is linked to a stronger steering flow that enhances the westward shift of the WPSH, preventing TCs from being active over the open ocean.

In addition to the direct role of steering flows in controlling TC lifetime, several other factors can also play a role in altering TC lifetime over the WNP basin. For example, recent studies by Wu and Wang (2004), Murakami et al. (2011), and Yokoi et al. (2013) proposed how TC tracks may be shifted due to changes in TC formation location and related this change in genesis location to TC lifetime variability. Indeed, Wu and Wang (2004) found that large-scale circulation and TC genesis location are two confounding factors that impact the northeastern shift of TC tracks during 2030–59. In this regard, any shift in TC genesis location toward the central WNP or changes in large-scale steering flows can be responsible for the shift in TC track curvature. This mechanism was supported by a study of Colbert et al. (2013), which showed a decreasing trend in the number of westward-moving TCs [~(4%–6%)] and an increasing trend in the ocean-recurving TCs [~(5%–7%)], as well as a weakening of the mean atmospheric circulation that causes fewer TCs to make landfall.

From the climate perspective, the above changes in TC steering flow or genesis location are ultimately related to dominant climate modes such as El Niño–Southern Oscillation (ENSO), Pacific decadal oscillation, or other ocean–atmosphere teleconnections (Wang and Chan 2002; Zhao et al. 2010; Camargo et al. 2007a; Zhao and Wu 2014). These large-scale climate modes can affect tropical circulations, monsoon troughs, upper-tropospheric troughs, the intertropical convergence zone (ITCZ), or WPSH, which in turn shape TC climatology. With a strong variability of these large-scale climate modes in all future projections (see, e.g., He and Zhou 2015; Zhang and Delworth 2016; Cai et al. 2021), quantifying their impacts and relationship with TC lifetime changes is, however, challenging. For example, Liu et al. (2014) ran an ensemble of experiments based on output from phase 5 of the Coupled Model Intercomparison Project (CMIP5) and found that the WPSH tends to be wider and shifting more to the west as it strengthens. However, He and Zhou (2015) found no significant changes in WPSH intensity in their CMIP5 analyses, with half of their model projections showing an intensification of WPSH, while the rest displayed a weakening.

Given various uncertainties in projecting TC lifetime, this work aims to better quantify how TC lifetime changes in the future climate for the WNP basin. To this end, we dynamically downscale the global Community Earth System Model (CESM) climate projections to examine the underlying physical mechanisms that drive the changes in TC lifetime under different hypothetical climates. This focus on physical understanding instead of any particular anthropogenic-forcing scenario can provide important insights into the overall TC activity projection and variability in the WNP basin, which we wish to present in this study.

The rest of this study is organized as follows. Section 2 describes our experimental design, input data, and model configuration for downscaling the CESM output for baseline and future scenarios. In section 3, model downscaling validation for the baseline period is presented from several different angles. The future projection of TC lifetime is then documented in section 4, and a summary of key findings is provided in section 5.

2. Experimental design

The future projection of TC climatology based on climate modeling is generally carried out in two different ways. The first is to use global climate models (GCMs) at a sufficiently high resolution to simulate the atmosphere–ocean interaction during TC formation and distribution. This approach can take into account global dynamics and coupling across components and scales, but it requires a large computational resource and storage that are not always accessible to users. Thus, a tradeoff between the model resolution, the duration of simulations, and the model complexity is often expected. In addition, there exist ad hoc basin-dependent characteristics of TC climatology that global models may not capture at present (e.g., Kim et al. 2014; Vecchi et al. 2019; Liu et al. 2019; Kieu et al. 2023). For example, Murakami et al. (2011) used the 20-km-resolution Meteorological Research Institute (MRI) atmospheric general circulation model (MRI-AGCM) to study TC climatology and future projections. Their model simulations could capture very strong TCs and a realistic TC distribution,

but the future period covered only a 25-yr period due to limited computational capacity. In addition, Also, some detailed TC inner-core structures are coarsely resolved at the 20-km resolution, making it difficult to evaluate the TC intensity climatology.

The second method, known as regional dynamical downscaling, initializes high-resolution regional climate models (RCMs) using initial and boundary conditions from coarser-resolution global models (Knutson et al. 2007, 2010; Hill and Lackmann 2011; Redmond et al. 2015). This approach is capable of producing much more detailed information on TC structure and climatology within a given region at a fraction of the computational cost of running a high-resolution GCM at the same resolution. With the advantage of lower computational cost and a much higher resolution, RCM downscaling is a powerful approach for studying projections of TC activities, especially when customized for some specific local areas.

Among many RCMs, the Weather Research and Forecasting (WRF) Model has been widely employed to investigate TC variability across temporal and spatial scales. For example, Jourdain et al. (2011) ran the WRF Model at a horizontal resolution of 35 km and showed that the model could capture reasonably both the seasonal and spatial distributions of TC genesis frequency comparable to the Joint Typhoon Warning Center (JTWC) best track data. Similarly, Jullien et al. (2014) used a coupled atmosphere–ocean WRF-ROMS model and noticed that their regional downscaling could provide reliable statistics of TC climatology and reproduce TC structure and air–sea exchange processes over the South Pacific during 1979–99. Kim et al. (2015) and Jin et al. (2016) likewise confirmed that WRF downscaling could indeed capture the observed spatial distribution and the interannual variability of TC activity.

It should be noted that regional downscaling is generally effective in simulating various extreme features, even with a relatively coarse resolution. This is because regional models such as the WRF Model include various detailed physical parameterizations that are often simplified in global models for climate simulations. In fact, Kim et al. (2015) or Jin et al. (2016) showed that WRF downscaling could reproduce large-scale TC climatology in the WNP basin, even with a 50-km horizontal resolution. Of course, such a 50-km resolution is insufficient in simulating category 4–5 TCs. However, the suite of WRF Model physics suitable for TC simulations could still allow the WRF Model to better capture some main TC characteristics in their studies, which are absent in global climate models.

a. Model configuration

In this research, the WRF Model version 3.9 (Skamarock et al. 2008) was used to downscale TC climatology for a baseline period and a range of future scenarios. The model domain was configured with 900 × 720 grid points in the west–east and north–south directions, which covers all the western North Pacific Ocean and allows the model to capture the expected TC genesis and activity over the WNP basin (see Fig. 1). Unlike a common nested-domain configuration in previous studies, we adopted in this study a single homogeneous horizontal grid spacing of 9 km for all downscaling experiments. This use of a single homogeneous resolution is computationally expensive, yet it removes some issues related to the model resolution inconsistencies across nested domains (Giorgi and Mearns 1999; Denis et al. 2002). Thus, our downscaling experiments better capture the large-scale TC–environment interaction for examining key properties of TC climatology such as genesis distribution, intensity, lifetime, or frequency. As discussed in, e.g., Zhao et al. (2009) or Davis (2018), a grid spacing smaller than 10 km is generally needed to fully represent the eye dynamics of very strong TCs, which justifies our setting of 9-km resolution in this study.

Note that our direct downscaling from the 100-km global data to the 9-km regional WRF domain may introduce some uncertainties due to substantial interpolation during the initialization and boundary updates. This is, however, a trade-off that we have to make if we want to have a homogeneous high resolution over the entire regional domain. Technically, we can evaluate this interpolation issue in two ways: (i) using a larger domain with an intermediate resolution to help reduce the jump as a typical nested-domain setup employs or (ii) using a higher-resolution global input data. For both approaches, more storage to save the model output and additional computational resources to process high-resolution global input data/larger intermediate domain size will be needed, which is beyond our current capability. Without these additional experiments, we note, however, that climate downscaling is generally more of the boundary forcing problem than the initial condition problem. As such, potential initial condition errors due to interpolation will be herein assumed to quickly diminish after some initial adjustment such that the climate state will be mostly driven by boundary forcing. This underlying assumption is certainly a weakness of our model design, and so our results need to be taken with caution hereafter.

Corresponding to this 9-km horizontal resolution, 41 vertical levels from the surface to the top of the atmosphere at 50 hPa were also used, with no fixed upper boundary lid such that vertical wave propagation can radiate away without vertical reflection. All simulations were conducted with the same set of physical parameterization schemes as in Vu et al. (2021) (hereafter noted as V21) including (i) a modified version of the (Kain and Fritsch 1990) cumulus parameterization scheme; (ii) the Yonsei University planetary boundary layer parameterization with the Monin–Obukhov surface layer scheme; (iii) the Rapid Radiative Transfer Model scheme for both longwave and shortwave radiation, including the full seasonal cycle of shortwave radiation (Mlawer et al. 1997); and (iv) the Lin et al. (1983) cloud microphysical scheme. All experiments used a Eulerian dynamical core with a time step of 30 s. While these schemes were demonstrated to capture the TC main climatology under idealized conditions at a resolution of 27 km in V21, we note that these schemes were also commonly used in previous studies of TC climate downscaling (see, e.g., Kim et al. 2015; Jin et al. 2016). As such, they are used herein with some potential caveats that the model outcomes may depend on these specific schemes. A more thorough approach to address this issue is to use a range of model

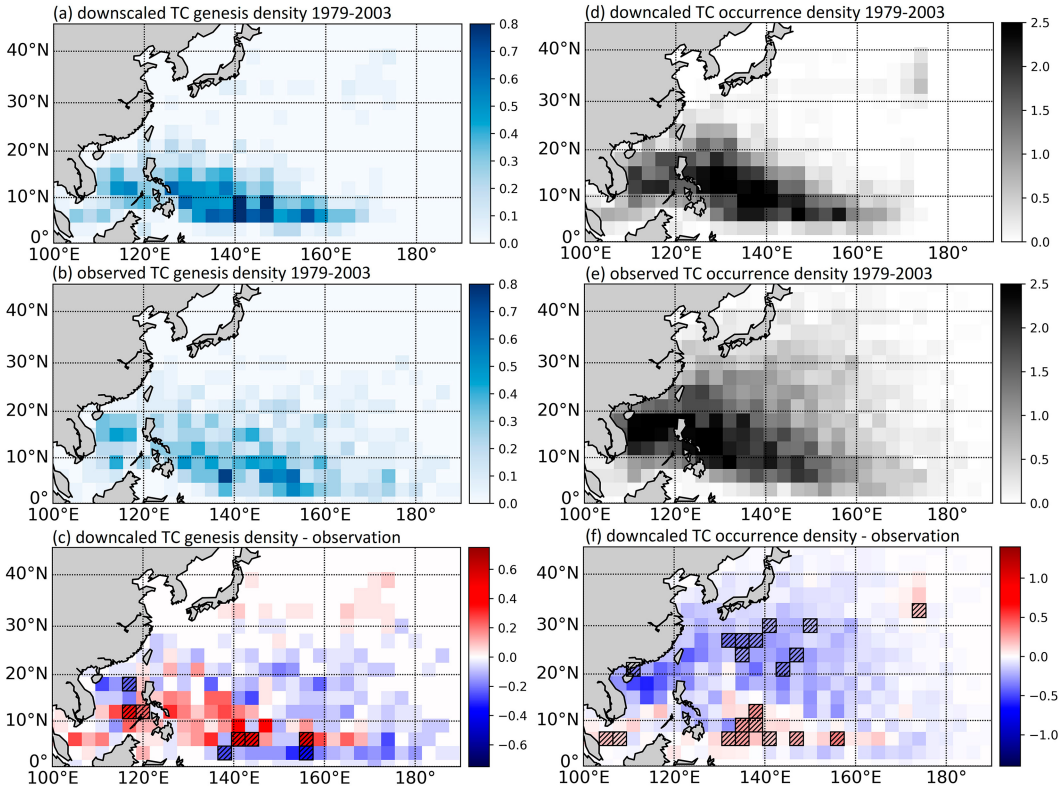

FIG. 1. Mean TC genesis rate (per year) from May to December during the period of 1979–2003 in the WNP basin for (a) WRF baseline downscaling simulations, (b) the JTWC data, and (c) the difference between WRF simulations and observed TCF distributions. The hatched boxes in (c) indicate significant differences in the means at the 0.1 level when using a two-tailed *t* test. (d)–(f) As in (a)–(c), but for averaged TC occurrence passing through each location.

physical parameterization schemes, which can help increase the robustness of model results. These sensitivity experiments are, however, expensive to run for the downscaling at the 9-km resolution. Thus, we will consider the use of different future periods and CMIP5 scenarios herein as an alternative way to address the robustness of our results.

b. *Input data*

For the initial and boundary conditions for the WRF Model, we used global gridded output from the CESM (Hurrell et al. 2013) experiments under the CMIP5 project (Taylor et al. 2012) at 1.0° × 1.0° (≈110 km × 110 km). This CESM dataset has been widely used and proven skillful in reproducing climatology for a range of seasonal, subseasonal-to-decadal scales (Richter et al. 2020; Yeager et al. 2018; Kirtman 2014). By default, these CESM data are archived at 26 pressure levels and 6-h intervals for all variables, and it already conforms to the input requirement to initialize the WRF Model. Note that these CESM global data have been bias corrected, using the 1981–2005 ERA-Interim reanalysis and following the methods described in Bruyère et al. (2014). The boundary condition bias correction approach is essential for TC downscaling, as it helps improve many metrics of RCM downscaling performance (Christensen et al. 2008; Warner et al. 1997; Bruyère et al. 2014). In addition to this important bias correction, we note that the CESM dataset is available in an intermediate format that can be used readily for the WRF Model. As such, the CESM data were chosen in our downscaling study.

For the purpose of dynamical downscaling, we carried out one baseline simulation during the twentieth century and two concomitant representative concentration pathway (RCP) future scenarios—namely RCP4.5 and RCP8.5—for the twenty-first century. These two future scenarios were chosen to maximize the difference between the more extreme and more conservative future scenarios within the CMIP5 framework. We validate the overall performance of our downscaling during the baseline period (1979–2003) against best track data over the WNP from the JTWC. This JTWC best track dataset includes TC location and intensity at 6-h intervals and a maximum sustained surface wind speed of 35 kt (1 kt ≈ 0.51 m s^{-1}) or above during the entire TC life cycle, which is needed to compute TC lifetime and compare with WRF output in this study.

While there are several different TC datasets in the WNP area, a study by Wu and Zhao (2012) suggested that JTWC could generally perform better in reproducing TC intensity over the period 1975–2007 as compared to other datasets in WNP such as the one from the Regional Specialized Meteorological Centre or the Shanghai Typhoon Institute. Chan (2008) also concluded that JTWC is a reliable source in terms

TABLE 1. A list of experiments conducted in this study.

Experiment	Period
Baseline	1979–2003
RCP4.5 midcentury	2030–50
RCP4.5 end of the century	2080–2100
RCP8.5 midcentury	2030–50
RCP8.5 end of the century	2080–2100

of TC intensity record, especially during the satellite era. Thus, we chose the 1979–2003 period for our baseline simulation, which could ensure the quality of TC records in the best track dataset in the WNP basin.

c. Simulation design

Given the aim of understanding future changes in TC lifetime relative to the PD climatology (often referred also to as the baseline simulation in previous studies), it is important to have first a good PD simulation that can capture key basinwide TC characteristics including intensity, lifetime, geographical genesis distribution, the seasonal cycle, and the interannual variations during the baseline period. For this, we conducted a baseline simulation in which the WRF Model was initialized annually from 0000 UTC 1 May to 0000 UTC 1 December for the 1979–2003 period. This 25-yr length of this baseline simulation suffices to validate the overall statistics of TC climatology and its seasonality for our WRF Model configuration.

With the baseline period as a reference, the next step to examine possible changes in TC lifetime is to carry out future simulations. Specifically in this study, two future periods including the middle of the twenty-first century (2030–50) and the end of the twenty-first century (2080–2100) within each RCP4.5 or RCP8.5 scenario were downscaled (see Table 1). This choice of the future 20-yr periods ensures that we have a sufficiently long dataset to quantify the annual variability of TC lifetime for each period, as well as robust epochal changes in TC climatology relative to the baseline period.

For both the baseline and future simulations, a TC-tracking algorithm as in V21 was applied, using standard thresholds that are customized to fit our 9-km resolution output. These thresholds include the minimum surface pressure, the maximum relative vorticity center, the 10-m wind speed maximum, the temperature anomaly at 400 hPa, and the TC minimum lifetime. Details of all TC-tracking criteria are summarized in Table 2.

Note that we employ in this study the continuous downscaling approach with lateral boundary conditions updated from global input every 6 h during each year of simulations, instead of reinitializing the downscaling experiments at a given interval as in Qian et al. (2003), Kotlarski et al. (2012), and Lucas-Picher et al. (2013). This continuous downscaling is important for our TC simulations, because reinitializing the model too frequently such as daily or weekly periods will take some initial time to spin up the WRF Model, resulting in an unexpected discontinuity in tracking TCs and related life cycles for our analyses. As such, our downscaling simulations are initialized only on 1 May of each year such that the WRF Model can maintain its continuous evolution of large-scale flows via lateral boundary controls.

3. Downscaling validation

a. TC genesis distribution

Before examining future projections of TC lifetime, it is necessary first to evaluate the downscaled TC climatology during the baseline period. Good performance during the baseline period helps to ensure that the model setting and physical options are well tuned for our downscaling study. For this purpose, Fig. 1 displays the observed TC genesis frequency (TCF) derived from JTWC data, along with the TCF obtained from the baseline simulation during 1979–2003. Here, TCF is defined as the total number of TC genesis events within a box of 5° × 5° divided by the total number of TCs detected within the 1979–2003 period. At 9-km resolution, one can see in Fig. 1 overall that the WRF downscaling can reasonably reproduce the observed spatial distribution of TCF, with a spatial correlation between the downscaled and observed distributions of 0.76 over the entire WNP basin. In addition, most TC formation occurs within the monsoon trough and the convergence zone, similar to the observed distribution. Of note, the two local maxima of TCF over the western part of the Philippines Sea (135°–145°E) and South China Sea (SCS; 115°–120°E) can be also seen in both the observed and downscaled climatologies.

A more detailed comparison of the downscaled and observed TCF shows that there are still some discrepancies in terms of the exact locations and magnitudes of the TCF centers in both the SCS and the East Philippines Sea, with the downscaled TCF centers shifted slightly more to the south in both regions. In addition, the WRF simulation tends to overestimate the total number of TCs, with 765 TCs detected from the WRF simulations as compared to 718 TCs recorded in the JTWC dataset during the baseline period (compare Fig. 2). Such dominant bias patterns in the TCF distribution with a negative/positive region to the north/south of the WNP basin are also realized for TC occurrence, which is defined to be the average number of TC passages at each location similar to TCF (Figs. 1d–f). These biases are somewhat expected, because TC activity in the SCS and the nearby Philippines Sea

TABLE 2. Criteria for tracking TCs from the 9-km resolution downscaling, using the WRF Model output.

Lat range	Gale-force wind ($m\ s^{-1}$)	Min pressure threshold (hPa)	Storm outer size (km)	Max distance between P min and vorticity centers (°)	Temp anomaly at 400 hPa (K)	Duration (days)
[40°S–40°N]	17.5	1004	300	5	3	3

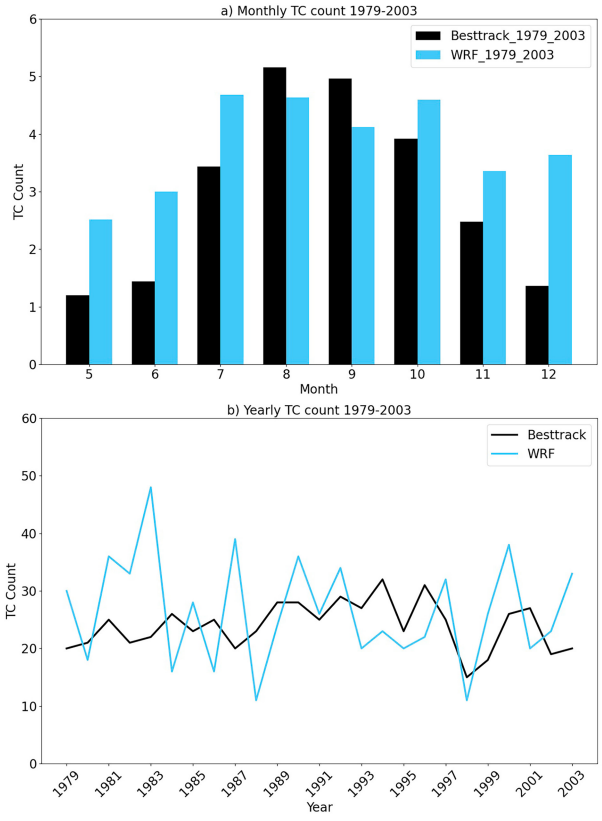

FIG. 2. (a) Seasonal distribution of TC genesis events as obtained from the WRF downscaling (cyan) and JTWC (black) during the baseline period and (b) time series of the annual TC genesis events during 1979–2003.

regions is generally difficult to model. These regions are either strongly modulated by monsoon activities or characterized by semienclosed areas bounded by landmass and islands. Thus, TCs forming in these subregions are often relatively short lived (Dao and Yu 2022) or are governed by abnormally strong monsoon troughs that are challenging to model as reported in, e.g., Tulich et al. (2011), Jin et al. (2013), and Kim et al. (2015).

The TCF or occurrence biases seen in Fig. 1 are ultimately linked to the WRF Model as well as the CESM input data (e.g., Murakami et al. 2014; Camargo 2013; Yokoi et al. 2012). The relative contribution of the global input data and the regional WRF configuration to these biases can be isolated by using different global inputs or changing model physics and/or vortex-tracking criteria. In fact, by varying the vortex-tracking criteria or using, e.g., CMIP6 input data, we can reduce the biases in the total number of TCs to match the observed number of TCs during the baseline period (not shown). For the purpose of calibrating the model performance that focuses on TC lifetime in this study, we, however, optimize our model configuration and the vortex tracking such that the downscaled TC lifetime can fit best to the observed lifetime during the baseline period (see Fig. 4), instead of TCF or occurrence. This is an important point, because any dynamical downscaling always contains different sources of model errors and biases. Thus, calibrating the downscaled TC climatology based on one metric will generally cause biases in other metrics that one has to compromise. In this regard, the biases in the TCF or occurrence distribution are to some extent unavoidable and a trade-off that we have to make for our TC lifetime focus, regardless of what global input or regional model settings one employs. Despite these biases in the TCF location and magnitude, the fact that the WRF Model can still capture the overall TC genesis and occurrence distribution with a high spatial correlation to observation is noteworthy, as it provides some fidelity in terms of the baseline TC climatology as expected for validation purposes.

b. *TC internal variability*

For TC frequency, Fig. 2 compares the monthly distribution and the annual variability of TC counts between the WRF downscaling and the JTWC data. One notices from Fig. 2a that the WRF Model can capture the seasonality of TC variability, with the peak activities during July–September as observed (correlation ≈ 0.82). Nevertheless, the WRF downscaling tends to produce more TCs during the early season (May–June) and the late season (November–December). This TC overestimation appears to be systematic and inherent to the CESM input data rather than related to the WRF Model, because similar behaviors were also reported in Murakami et al. (2011). In fact, this excess of TC formation during the early and late seasons is the main cause for the larger TCF shown in Fig. 1.

One could in principle improve this bias in TC seasonality by using different WRF Model physics, global input data for downscaling, or vortex-tracking thresholds. However, these approaches do not change the fact that improving one aspect of TC climatology would adversely affect other aspects of TC climatology. With our focus on TC lifetime, the bias in TC seasonal distribution is again another trade-off that we have to make.

Similar to the seasonality, the WRF downscaling could capture some interannual variability of TC frequency during the baseline period, with a correlation between downscaling and observation of ≈0.3. However, few details of simulated interannual variability such as the strong fluctuation during the early period from 1979 to 1983 are not observed in the best track data. On average, the WRF downscaling produces 26.5 TCs per year as compared to ~24 recorded in the JTWC data. These higher TC annual numbers are consistent with the fact that more TCs are produced during early and late seasons as seen in Fig. 2a and the higher TCF shown in Fig. 1a. Of course, these biases in TC annual time series or the seasonal distribution in Fig. 2 may change for different WRF Model configurations or vortex-tracking algorithms. However, with our main calibrations of the WRF downscaling to optimize the model performance for TC lifetime, these biases are expected to exist regardless of what model settings, global input data, or tracking algorithms are used.

Along with TC frequency, our downscaling settings also capture a range of TC intensities at the 9-km resolution,

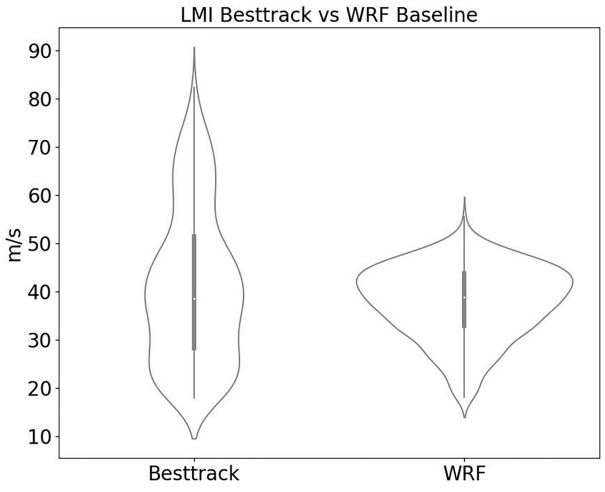

FIG. 3. Violin plot showing distributions of the TC LMI obtained from (left box) the JTWC data and (right box) the WRF downscaling during the baseline period from 1979 to 2003. Each box shows the 25th and 75th percentiles, the median (red lines), and the maximum and minimum values (black bars) of the LMI distributions.

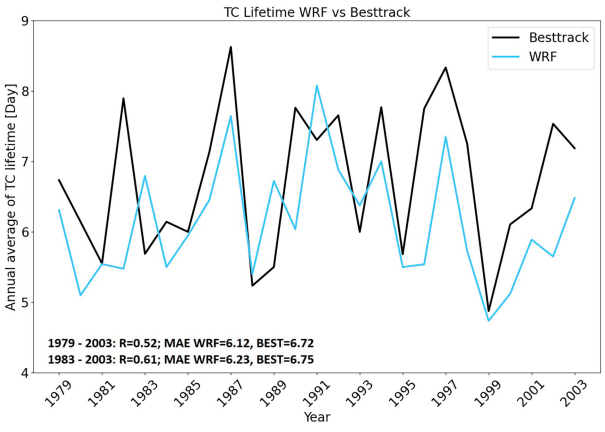

FIG. 4. Annual average of TC lifetime during 1979–2003. The blue line corresponds to the best track JTWC data, while the black line is obtained from the downscaled baseline simulations.

which allows us to track TCs effectively. Among different TC intensity metrics, the TC lifetime maximum intensity (LMI) is of importance, because it does not depend on vortex-tracking algorithms, and so it is a good metric to validate the downscaling performance. In this regard, Fig. 3 compares the LMI statistics between the WRF downscaling and JTWC during the baseline period. Overall, the downscaled LMI median is comparable to that obtained from the best track, thus confirming the capability of the WRF Model in simulating TC intensity. Of course, there is a gap between the downscaled upper quartile and the outliers due to the model limitations related to, e.g., different approximations or parameterizations of physical processes in the WRF Model. As such, the WRF Model still cannot capture the very high-intensity statistics even at the 9-km resolution as shown in Fig. 3, similar to previous studies (e.g., Knutson et al. 2008; Murakami and Sugi 2010; Tsou et al. 2016). Note that this issue with simulating very intense TCs should have little impact on our examination of TC lifetime herein, because TC lifetime statistics depend more on the entire TC life cycle instead of the maximum intensity at one point in the TC life cycle.

c. *TC lifetime*

Regarding the statistics of TC lifetime in our WRF downscaling, Fig. 4 shows how the WRF Model can simulate TC lifetime during the baseline period as compared to the JTWC best track data from 1979 to 2003. Here, the lifetime is defined as the total duration of a TC from a genesis point where its wind speed is >17.5 m s^{-1} to a final dissipation stage where its wind speed is <17.5 m s^{-1} as detected by the vortex tracker or a landmass point is reached at any stage of the TC life cycle. With the aim of calibrating the WRF downscaling to best simulate TC lifetime, the time series of the annual average WRF-simulated TC lifetime during the baseline period could indeed compare well to that obtained from the best track data in terms of the annual variability and magnitude, with a correlation coefficient of 0.52. The correlation between the downscaled and observed TC lifetime is even higher during a later period (1983–2003), reaching a value of 0.61 at a 95% significant level despite an overall higher mean lifetime in the best track.

Consistent with the overall TC genesis distribution, TCs with a longer lifetime tend to form in the East Philippine Sea, while those forming in the SCS tend to have a shorter lifetime (Fig. 5). In the WRF downscaling, we notice that the longest lifetime is for TCs forming in the far east of the WNP (between 140° and 160°E), yet the observed long-lifetime TCs are somewhat closer to the East Philippine Sea (between 135° and 155°E). Because of this TC lifetime distribution, the biases in TC genesis density as seen in Fig. 1 may impact TC lifetime by producing more or less TCs with different lifetimes in those bias areas. Although there is no simple way to account for the effects of TC genesis biases on TC lifetime, we note that all of our TC lifetime assessments hereafter will be computed for a basin average. As such, the biases in TC formation distribution are expected to have a minimum impact on the climatic change in TC lifetime. As seen in Figs. 4 and 5, the WRF downscaling could indeed demonstrate the overall distribution as well as the annual variability of TC lifetime during the baseline period as needed for our subsequent analyses.

Similar to the total TC count, the downscaled TC lifetime is generally dependent on the model physics, resolution, or vortex-tracking criteria. While some metrics such as the TC LMI are less sensitive to vortex-tracking algorithms, TC lifetime generally depends on how a vortex is detected from the model output. For example, stricter TC-detection thresholds generally result in a smaller number of TCs and a shorter lifetime. Based on sensitivity analyses, our vortex-tracking criteria listed in Table 2 provide the best TC lifetime statistics in terms of its correlation with the observations, despite a higher total TC count, mostly short-lived TCs <3 days, or the far-east distribution of TCF as seen in Figs. 2 and 5. The fact that the averaged TC lifetime variability obtained from the WRF

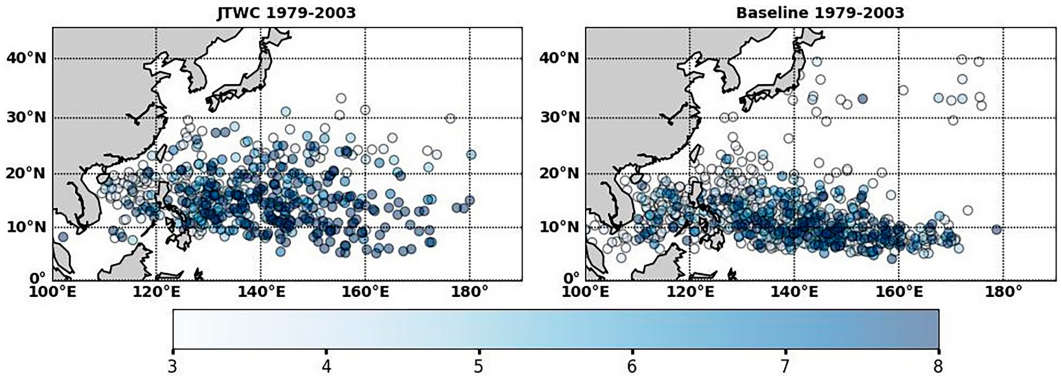

FIG. 5. Distributions of TC lifetime (shaded) associated with the corresponding genesis location during 1979–2003 as obtained from (left) the best track JTWC data and (right) the WRF baseline simulations.

simulation is comparable to the observed TC lifetime suggests that our model settings can provide useful TC lifetime climatology and related changes that we wish to examine for future climate scenarios in this study. So long as these same criteria are applied to future periods, the relative changes between the baseline and future periods can still be meaningfully evaluated as presented in the next section.

4. Future projection

a. TC lifetime projection

To have a broad picture of TC projection in the WNP basin under the RCP4.5 and RCP8.5 scenarios, Fig. 6 compares first the epochal changes in TC statistics for LMI and TC lifetime between the midcentury (2030–50) and the end of the century (2080–2100) relative to the baseline period. One notices a significant increase in LMI across the future scenarios, with the future LMI median in the range of 45–47 as compared to ~40 m s^{-1} in the baseline simulations. Such an increase in LMI is consistent with the warming scenarios in RCP4.5 and RCP8.5 and agrees with previous modeling studies (e.g., Yoshimura et al. 2006; Walsh and Ryan 2000; Tsou et al. 2016). Looking at the 75th percentile and the maximum outliers, we observe also that there are more intense TCs, with several outliers reaching category 5 in all future scenarios. This confirms the WRF Model's response to future warming in terms of TC intensity variability and development needed for further analysis.

Unlike the LMI projections, the epochal changes in TC lifetime do not show any noticeable trend relative to the baseline period. Specifically from the full lifetime distribution, both the median and the upper or lower percentile of TC lifetime exhibit a similar magnitude of ≈3.8, 10, and 3.7 days among all future periods and scenarios as compared to the baseline average. Note, however, from the outliers in Fig. 6 that there emerge now some very long-lived TCs in all future simulations. These outliers suggest some potential changes in the tail of the TC lifetime statistics that is not clearly seen in Fig. 6.

To have more insights into these outliers of TC lifetime in the future, Fig. 7 shows the normalized probability distribution of TC lifetime, along with a close-up of the tail of the

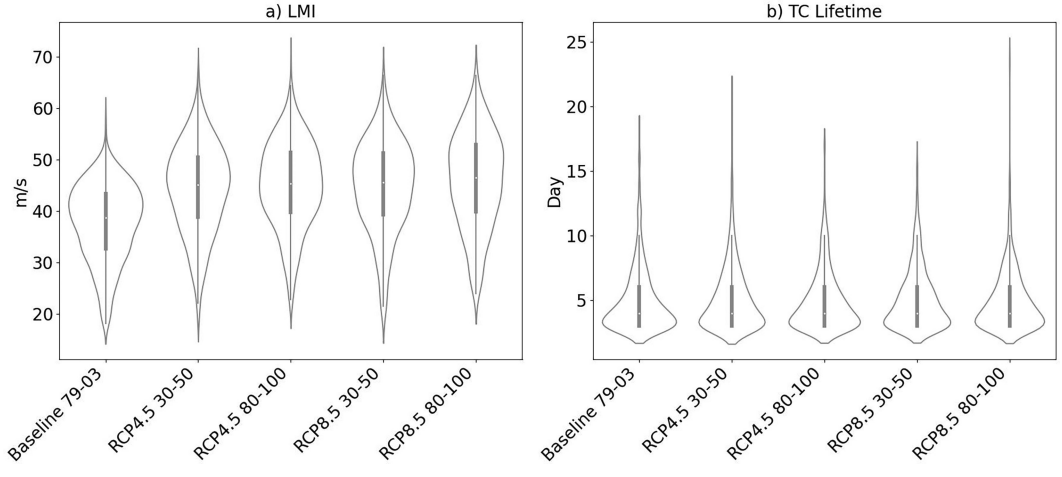

FIG. 6. Violin plots of the 20-yr statistics of (a) TC LMI (m s^{-1}) and (b) TC lifetime (day) for the baseline period and two future scenarios RCP4.5 and RCP8.5. Included in these box plots are the 25th and 75th percentiles, the median (red line), and the maximum and minimum values for the outliers.

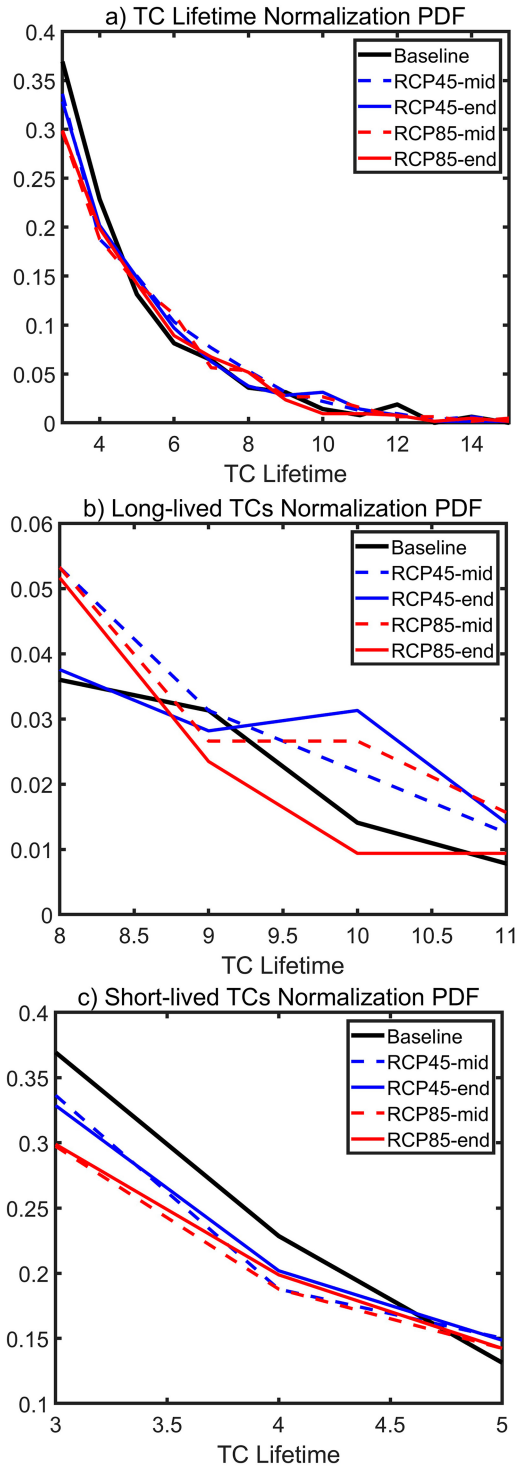

FIG. 7. Normalized probability distribution function (PDF) obtained from the WRF baseline simulation (black), RCP4.5 midcentury (blue dashed), RCP4.5 end of the century (blue solid), RCP8.5 midcentury (red dashed), and RCP8.5 end of the century (red solid) for (a) all TCs and a closeup of the PDF tail for (b) long-lived TCs and (c) short-lived TCs.

distributions for short-lived and long-lived TCs. While there is no significant change in the TC lifetime median as seen in Fig. 6, the frequency distribution of TC lifetime displays more frequent long-lived TCs (i.e., TC lifetime is between 8 and 11 days; Fig. 7b) across all scenarios. Likewise, the short-lived TCs (i.e., TC lifetime is 3 to <5 days) also show more noticeable changes in the future, with fewer short-lived TCs in all scenarios as compared to the baseline period (Fig. 7c). An additional statistical test for these differences in the number of long-lived and short-lived TCs between the baseline and the future confirms that the increase/decrease in the long-lived/short-lived TCs is significant with p value < 0.05 (using the Student's t test).

The only exception for this change in the tails of TC lifetime distribution is for RCP8.5 toward the end of the twenty-first century, which shows a slightly different behavior with fewer long-lived TCs despite capturing several extreme cases of very long-lived TCs seen in Fig. 6. This different behavior of the end-century RCP8.5 could be related to the well-documented characteristics of TC projection with fewer TCs overall in the warmest scenario (e.g., Knutson et al. 1998; Zhang and Wang 2017), which reduces the robustness of the statistics at the tail of the distribution. In addition, any future projection of TC characteristics is greatly influenced by various uncertainties such as future scenarios, model dynamics, or physical parameterizations (Tang et al. 2022; Huang et al. 2023). Regardless, the overall consistency of more long-lived TCs but fewer short-lived TCs in the warmer climate is noteworthy here, as it suggests that there must be some changes in the large-scale environment that affect TC lifetime, which we want to further investigate.

b. *TC lifetime and Niño-3.4 correlation*

As a first step to understand the changes in TC lifetime distribution, we examine some potential climate factors that can account for these lifetime changes. Among several possible large-scale relationships, ENSO appears to be the most apparent one, given that El Niño or La Niña years have a large effect on TC activities in the WNP (Wang and Chan 2002; Camargo and Sobel 2005; Chan 2000). For example, Wang and Chan (2002) and Camargo and Sobel (2005) showed that El Niño years tend to have higher accumulated energy, which implies more intense and longer-lived TC than in La Niña years. Similarly, Wang and Chan (2002) found that TC motion tends to shift northward during El Niño years, whereas it is displaced westward during La Niña years. These studies, however, focused on TC lifetime in the past climate that may or may not be extended to the future climate. For the purpose of examining how ENSO affects TC lifetime in our future periods, we use the same Niño-3.4 index as in previous studies, which is defined to be the SST anomaly averaged between (5°N–5°S, 170°–120°W) that is often used to monitor ENSO variability.

Figure 8 shows the time series of TC lifetime and the corresponding Niño-3.4 index for both the baseline period and all four future scenarios. For the baseline simulations, there exists indeed a positive correlation between WRF-downscaled TC lifetime and Niño-3.4 with a correlation as large as $r = 0.4$,

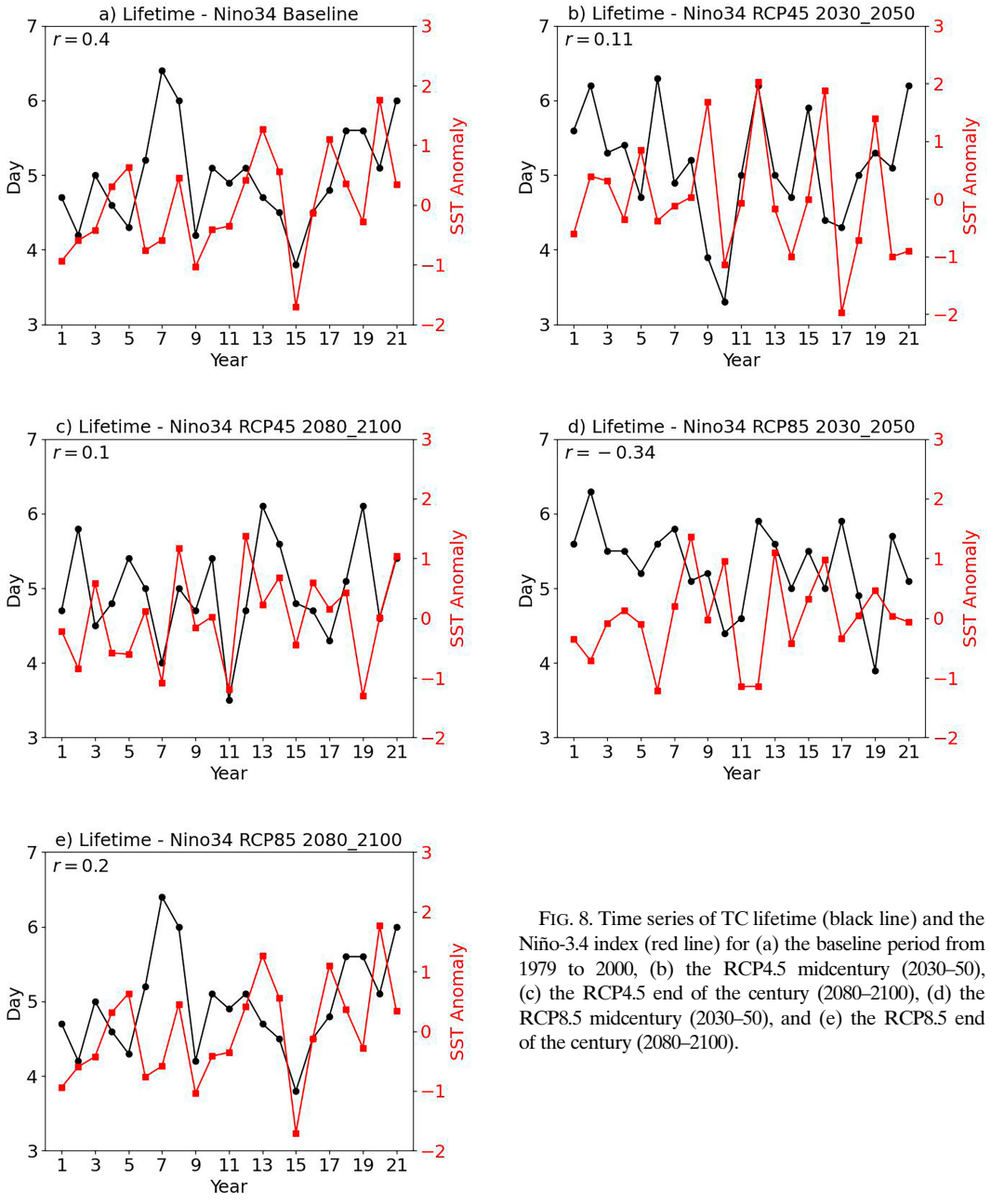

FIG. 8. Time series of TC lifetime (black line) and the Niño-3.4 index (red line) for (a) the baseline period from 1979 to 2000, (b) the RCP4.5 midcentury (2030–50), (c) the RCP4.5 end of the century (2080–2100), (d) the RCP8.5 midcentury (2030–50), and (e) the RCP8.5 end of the century (2080–2100).

which is also consistent with observational analyses in, e.g., Wang and Chan (2002), Camargo and Sobel (2005), and Kim et al. (2013). Practically, this correlation indicates that TCs tend to experience a longer lifetime during El Niño years, possibly because they possess a higher intensity, recurve north/northeastward, and travel over the warm ocean at a longer time before making landfall or moving into the colder midlatitude ocean as discussed in (Wang and Chan 2002; Yonekura and Hall 2011; Kim et al. 2013). This positive correlation obtained in our downscaling confirms our WRF configurations in capturing not only TC characteristics but also the large-scale environment in the WNP basin during the baseline period.

This relationship between Niño-3.4 and TC lifetime becomes, however, less apparent in all future scenarios, despite a significant correlation during the baseline period. As seen in Fig. 8, the Niño–TC lifetime correlation drops from 0.4 in the baseline experiment (Fig. 8a) to $r = 0.11$ in RCP4.5 2030–50 (Fig. 8b), to $r = 0.10$ in RCP4.5 2080–2100 (Fig. 8c), and to $r = 0.2$ in RCP8.5 2080–2100 (Fig. 8e). This correlation even becomes negative during 2030–50 in the RCP8.5 experiment; that is, El Niño year may imply a shorter TC lifetime in the

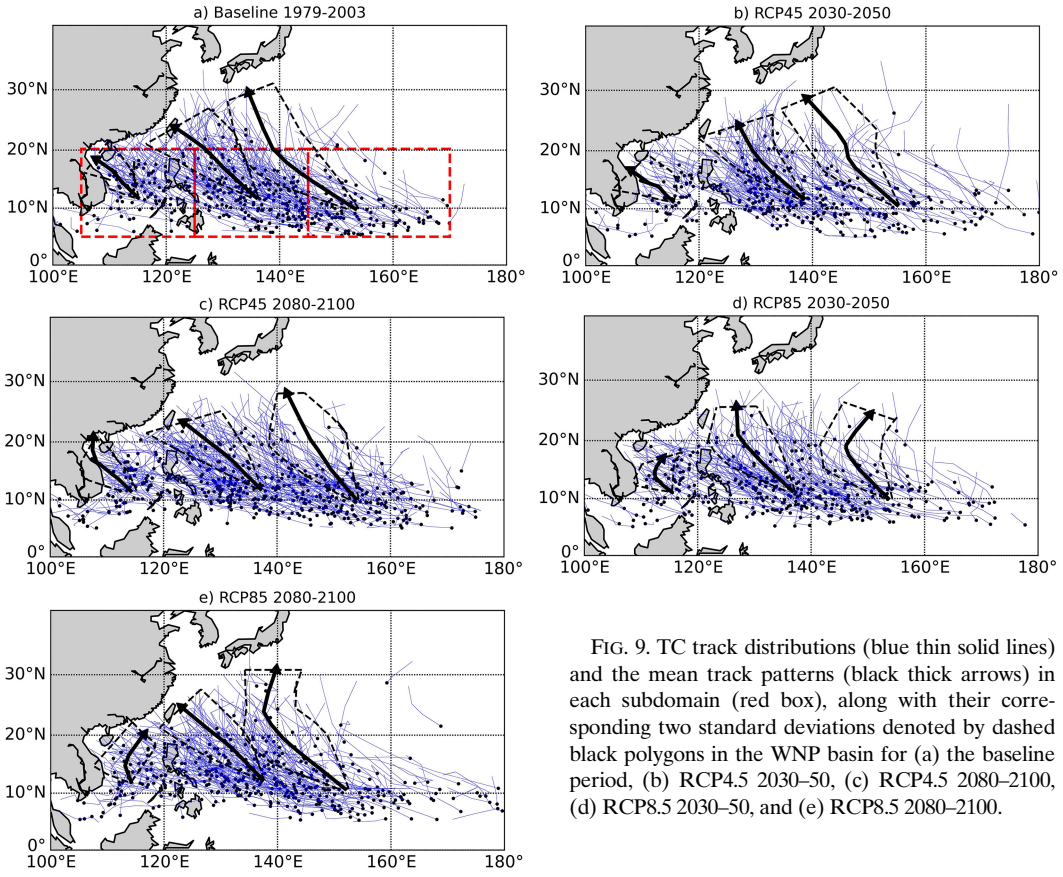

FIG. 9. TC track distributions (blue thin solid lines) and the mean track patterns (black thick arrows) in each subdomain (red box), along with their corresponding two standard deviations denoted by dashed black polygons in the WNP basin for (a) the baseline period, (b) RCP4.5 2030–50, (c) RCP4.5 2080–2100, (d) RCP8.5 2030–50, and (e) RCP8.5 2080–2100.

future. At face value, this change in the Niño–TC lifetime correlation suggests that other changes in large-scale environments such as the ITCZ, monsoon activities, tropical upper-tropospheric trough, or WPSH must occur and interfere with TC lifetime in the WNP. Thus, the ENSO3.4 index is inadequate for the problem at hand; it may not be capturing components of ENSO that are of interest to the current problem, or it is capturing confounding variations of other modes such as monsoon activities, the WPSH, or the ITCZ. In any case, the ENSO3.4 index cannot alone be used to predict changes in TC lifetime over the WNP. In the next section, we will look into several individual environmental factors that are directly relevant to TC climatology beyond the general ENSO index.

c. *Large-scale influence*

To explore other large-scale environments, we examine next the change in TC track patterns in different future scenarios and how this change is linked to TC lifetime. Figure 9 shows the spatial distribution of all TC tracks obtained during the baseline period and future runs. In general, TC tracks in the WNP basin can be categorized into three main prevailing directions as reported in the previous studies (e.g., Ho et al. 2004; Wu et al. 2005; Camargo et al. 2007b). Specifically, the first group of TC tracks [referred to as straight moving (SM)] consists of TCs that move over the SCS and to the southeast of Taiwan, with their main tracks moving westward. The second group [referred to as recurving landfall (RCL)] includes TCs that form to the east of the Philippine Sea and tend to move northwestward and affect the coastal region of East Asia. The last group [referred to as recurving ocean (RCO)] consists of TCs that recurve to the northeast along the edge of the WPSH. Visually, these three groups are relatively straightforward to identify in both the baseline and future simulations as displayed in Fig. 9 (see the thick black arrows). However, for the purpose of quantifying the change in the TC track distribution among different periods and scenarios, we define in this study these track categories based on their initial genesis location within [5°–10°N, 105°–125°E] for the SM group, [5°–10°N, 125°–145°E] for the RCL group, and [5°–10°N, 145°–170°E] for the RCO group.

Despite their gross similarity, a detailed comparison of the general track patterns among the future scenarios and the baseline period reveals some significant changes, especially for the RCL and RCO groups. This change is most apparent for the end-of-the-century scenarios (Figs. 9c,e), which show that future TCs tend to recurve more to the ocean instead of heading toward the south of Japan area as in the baseline period. For the RCL group, TCs are similarly shifted to the north of Taiwan, which is apparent even for the midcentury scenarios. Among all of the changes in TC track patterns, we note that the change in the RCO and RCL groups has the most significant effect on TC lifetime. This is because TC

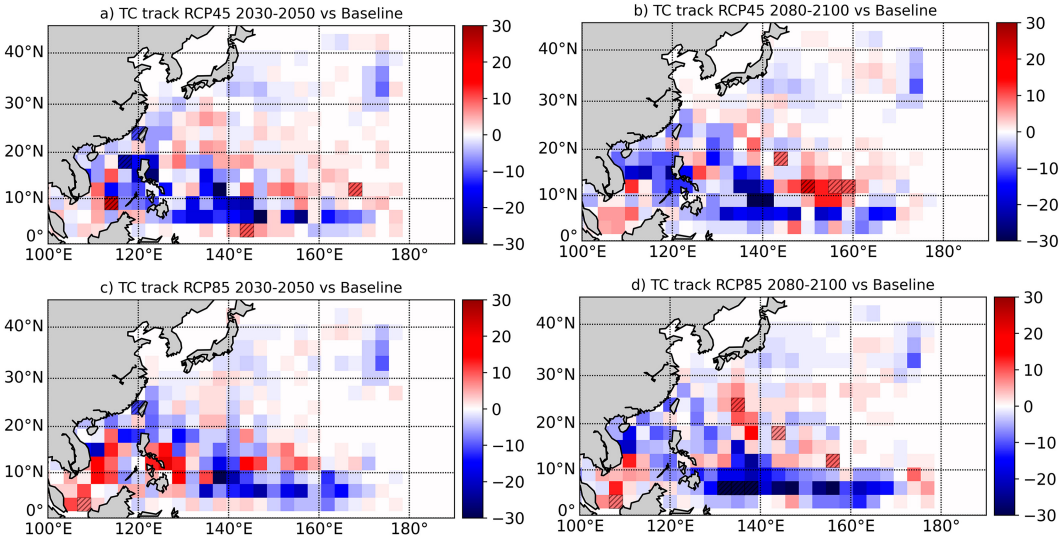

FIG. 10. The difference in TC track density between the baseline period and future scenarios including (a) RCP4.5 2030–50, (b) RCP4.5 2080–2100, (c) RCP8.5 2030–50, and (d) RCP8.5 2080–2100. The hatching boxes indicate the significant difference at a 90% confidence interval, using the Student's *t* test. Positive values indicate higher TC track density in the future as compared to the baseline period, and negative values indicate smaller TC track density.

tracks curving more to the open ocean imply that TCs will have more time to maintain their intensity, instead of making landfall that shortens their life as discussed in, e.g., Colbert et al. 2015 and Yokoi et al. 2013.

To quantify these track pattern changes beyond just the mean track directions, Fig. 10 shows the differences in TC track density between the baseline and future scenarios, for each 5° × 5° box over the WNP basin. Intuitively, these 5° × 5° track density boxes indicate how often TCs visit the boxes during the simulation, which is also mentioned as TC occurrence density in previous studies (Royer et al. 1998; C.-Y. Lee et al. 2020; Murakami et al. 2014). One notices in Fig. 10 that TC track density in the future is indeed higher over the open ocean (i.e., the red areas within [10°–30°N] × [140°–170°W]), while it is significantly less near the land and lower latitudes (the blue areas). In this regard, our future downscaling suggests that TCs tend to be more active over the open ocean under both the high- and low-emission scenarios, which explains the change in the tails of long-lived TC lifetime seen in Fig. 7.

Also of interest in Fig. 10 are the changes in TC landfalling, which can be seen as the difference in track density between the future and the baseline periods along the coastal areas. While examining landfalling TCs would introduce additional uncertainty due to the small sample size, one could notice that the Taiwan and Philippine areas show the most consistent changes, with overall reduced track density across future scenarios (except the RCP85 midcentury scenario over the Philippines). Other coastal regions such as Japan or Korea show less significant change with some alternating increase or decrease in track density. Note that track density for coastal storms may include both short-lived TCs forming near coastal regions, which are largely influenced by coastline topology and islands, and long-lived TCs traveling from far open ocean. Thus, it is difficult to separate if the changes in track landfalling are due to short-lived or long-lived TCs. However, the results shown in Fig. 10 could indicate the tendency of less TC track crossing over the Taiwan and Philippine areas in the future climate as obtained herein.

It should be noted that curving to open ocean alone is generally insufficient to ensure a longer TC lifetime, because it is possible that TCs may also move into regions with colder SSTs earlier and therefore have their lifetime shortened. To study this possibility, Fig. 11 compares the climatological averages of TC translation vectors between the baseline and each future simulation. Here, the mean TC translation vectors are calculated for each 2 × 2 grid box by taking the average of all TC motion vectors that passed through that box. As shown in Fig. 11, there is no clear trend in TC translation speed in all future scenarios, with an overall mixed change over the entire WNP. Given the more noticeable changes in the mean track directions as shown in Fig. 10, it is therefore more likely that TC translation speed plays a less significant role in the future changes in TC lifetime, compared to the change in the mean track pattern.

One could further quantify these changes in each group of TC track and translational direction by applying cluster analyses for TC tracks as obtained from the baseline and future scenarios as in Camargo et al. (2007a). This cluster analysis can help evaluate quantitatively the relative changes in the number of TCs, their genesis location, or track density within each cluster. These detailed analyses require, however, some additional cluster sensitivity and TC angle distribution to define TC clusters subjectively as discussed in Camargo et al. (2007a), which is, however, beyond the scope of our TC lifetime focus here, and so we will not pursue it further.

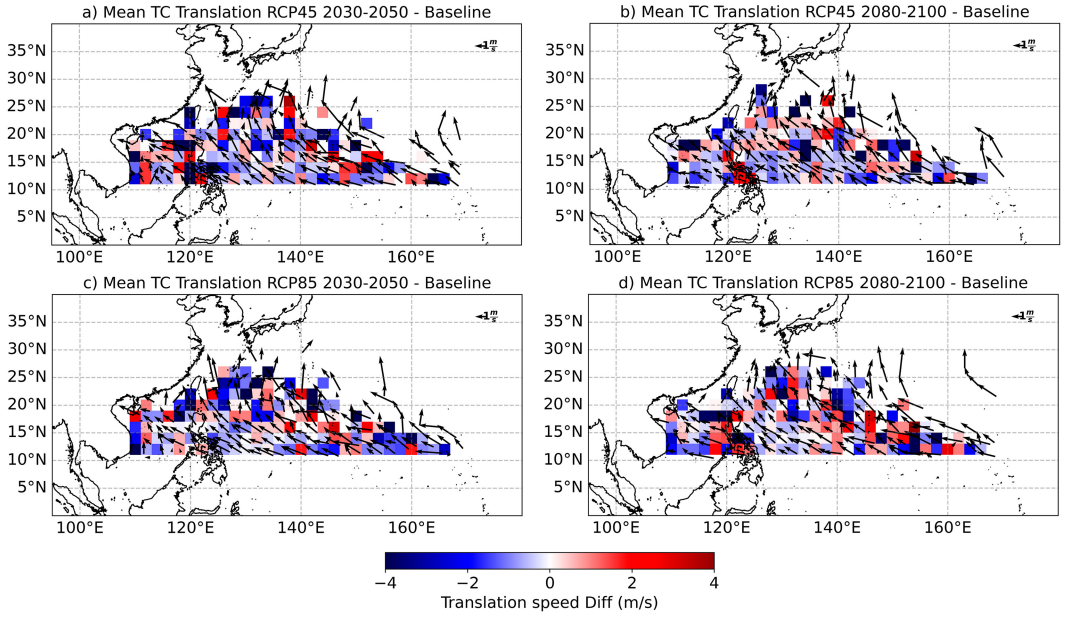

FIG. 11. The averaged difference in TC translation vectors relative to the baseline period for (a) RCP4.5 2030–50, (b) RCP4.5 2080–2100, (c) RCP8.5 2030–50, and (d) RCP8.5 2080–2100. Superimposed are the corresponding differences in TC translation speed (shaded; m s^{-1}).

From a larger perspective, a natural question is what are the possible causes for the changes in the TC mean track direction as seen in Fig. 9. Given that TC tracks are generally guided by environmental steering flows associated with large-scale circulations, any potential changes in TC track patterns should be linked to changes in the WPSH, which is the dominant large-scale system in the WNP basin (Tao and Chen 1987; Yihui and Chan 2005). From this perspective, any variability in the WPSH would immediately affect TC track patterns in the WNP basin, especially for TCs forming in the tropics that follow the western edge of the WPSH (Ho et al. 2004; Wu et al. 2005).

Given such a key role of the WPSH in TC track climatology, Figs. 12–14 compare the WPSH between four future scenarios and the baseline period for three summer months from July to August. Here, we follow Murakami et al. (2011) and plot the anomaly of monthly mean geopotential height at 500 hPa relative to the domain average during the entire simulation period to examine its variability in the future. It is of interest to notice from these figures that WPSH appears to be shifted more to the south during July but then retreats to the northeast during August and September in all future scenarios, especially toward the end of the century. Furthermore, WPSH also strengthens in the future as can be seen from the emergence of the 40-gpm anomaly contour in Fig. 12. Along with the above changes in the WPSH, we observe an enhanced westerly flow associated with monsoon troughs in the tropical region between [5°–10°N] × [120°–140°W]. As a result of this strengthening of the westerly flow, the prevailing TC westward motion in the main genesis area during summer months becomes slower in the future climate. In combination with the northeastward extension and higher strength of WPSH during August–September, TCs forming in the lower latitudes tend to drift more northwestward and stay over a warm ocean for a longer time in future scenarios, thus explaining the overall behaviors of the RCO track group in Fig. 9.

It should be noted that analyzing the WPSH for each month as shown in Figs. 12–14 generally introduces some uncertainty in the characteristics of the WPSH, as compared to the seasonal average used in previous studies. However, this monthly analysis is needed in our case here, because the prevailing TC track pattern changes every month during the main TC season in the WNP basin. For example, the dominant northwestward group tends to occur early in the season during July–August, but it tends to shift to north-northwest later in the season (e.g., Harr and Elsberry 1991; Camargo et al. 2007a). As such, providing the WPSH analysis for each month could help better see how WPSH affects TC track pattern as seen in Figs. 12–14. Note also that July–October is a period when TCs are most active in the WNP basin. As such, any variability of large-scale circulations during this time would have more impact on TC characteristics such as tracks and lifetime, which justifies our choice of the monthly WPSH analyses despite its larger uncertainty.

The future shifts of WPSH under different climate scenarios as obtained in our downscaling are not new, as they have been in fact documented in previous studies, albeit the future shifts are somewhat inconclusive in terms of location and magnitude. For instance, Liu et al. (2014) found that WPSH tends to be stronger and expands westward under scenarios RCP2.6, RCP4.5, and RCP8.5. On the other hand, He and Zhou (2015) showed that half of the CMIP5 models captured an enhanced WPSH, whereas the other half projected a weakening trend of WPSH under both RCP4.5 and RCP8.5. Of

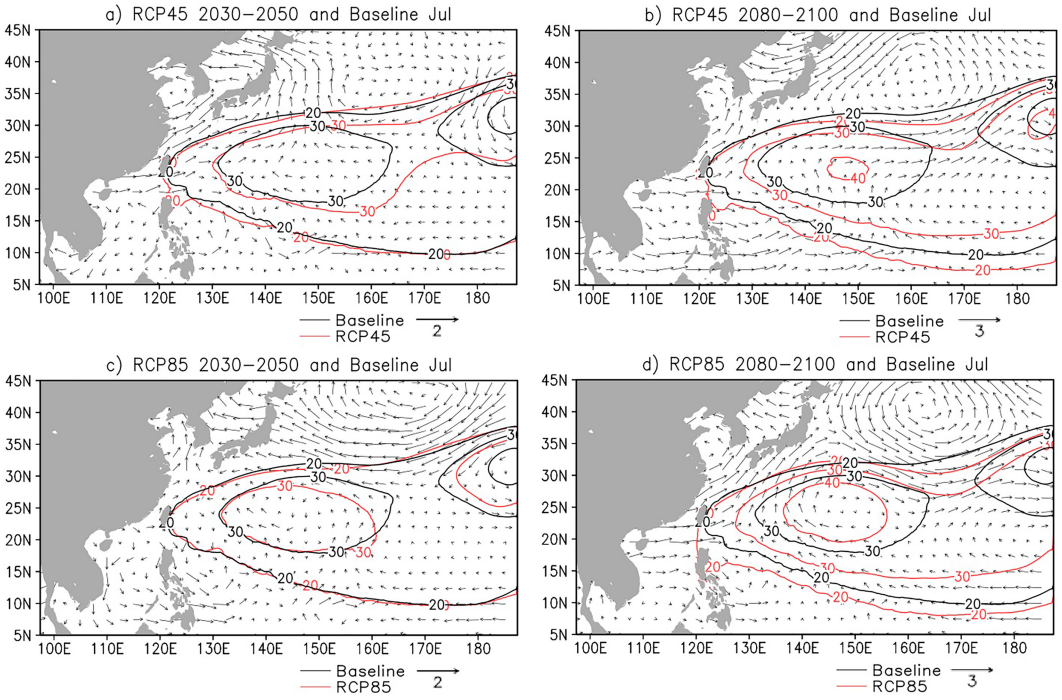

FIG. 12. The 20-yr average of geopotential height anomalies for the baseline period (black contour) and four future scenarios including (a) RCP4.5 2030–50, (b) RCP4.5 2080–2100, (c) RCP8.5 2030–50, and (d) RCP8.5 2080–2100 (red contour) during July. Superimposed is the difference in the steering flow (vectors) between each future scenario and the baseline period.

note is the result that WPSH can be strengthened by stronger descending associated with enhanced Hadley circulation due to warmer SST anomaly as discussed in, e.g., Wu and Zhou (2008) and Chung et al. (2011). This strengthening of the descending branch appears to differ from other modeling studies, which captured the weakening of the Walker and Hadley circulations under global warming scenarios (Lu et al. 2007; Vecchi and Soden 2007; Gastineau et al. 2009).

To further relate the changes in WPSH shown in Figs. 12–14 to the large-scale tropical circulation, Fig. 15 shows the mean profiles of averaged vertical motion within both the ascending and descending branches of the Hadley cell. Here, the ascending branch is defined as a 3° latitudinal zone that moves between 9° and 15°N during July–September, whereas the descending branch is defined to be a zone of the same width that shifts between 27° and 29°N during the same period.

Overall, the ascending branch is stronger in all future climates relative to the baseline, most noticeably at 300 hPa. Likewise, the descending branch of the Hadley cell is also consistently stronger across warmer climate scenarios and periods in our downscaling simulations. This behavior of the Hadley cell appears to be inconsistent with the projection that the future troposphere is more stable due to larger warming at the upper level than that at the lower level (e.g., Hill and Lackmann 2011). One possible explanation for this inconsistency could be related to the increase in the latent heating and precipitation as presented in, e.g., Su et al. (2014) and He and Zhou (2015), which results in enhanced ascending and descending branches of the Hadley circulation. Because of this, the upper cooling of the Hadley cell due to stronger vertical motion can be further enhanced, which increases the upper-level convergence. As a result, WPSH can be strengthened as seen in our simulations, despite a more stable troposphere. In this regard, our result is consistent with the findings of Su et al. (2014) and He and Zhou (2015) that the enhanced descending branch of the Hadley circulation under the warmer SST condition accounts for a stronger WPSH, which eventually affects TC track patterns as obtained herein.

5. Conclusions

In this study, future changes in TC lifetime in the western North Pacific basin were examined, using homogeneous high-resolution downscaling under the low and high greenhouse gas concentration pathways RCP4.5 and RCP8.5. Verification of TC main characteristics during a baseline period from 1979 to 2003 showed that our WRF downscaling could capture some key TC statistics such as seasonality and interannual variability as observed in the best track data. With some biases in TC statistics that we had to compromise when calibrating the WRF Model and the vortex-tracking algorithm for TC lifetime, our baseline verification showed that the dynamical downscaling of TC climatology must be properly optimized for a specific metric before one can start examining its future change. In particular, a good downscaling design for one aspect of TC climatology such as TC lifetime does not ensure that other aspects such as TC frequency

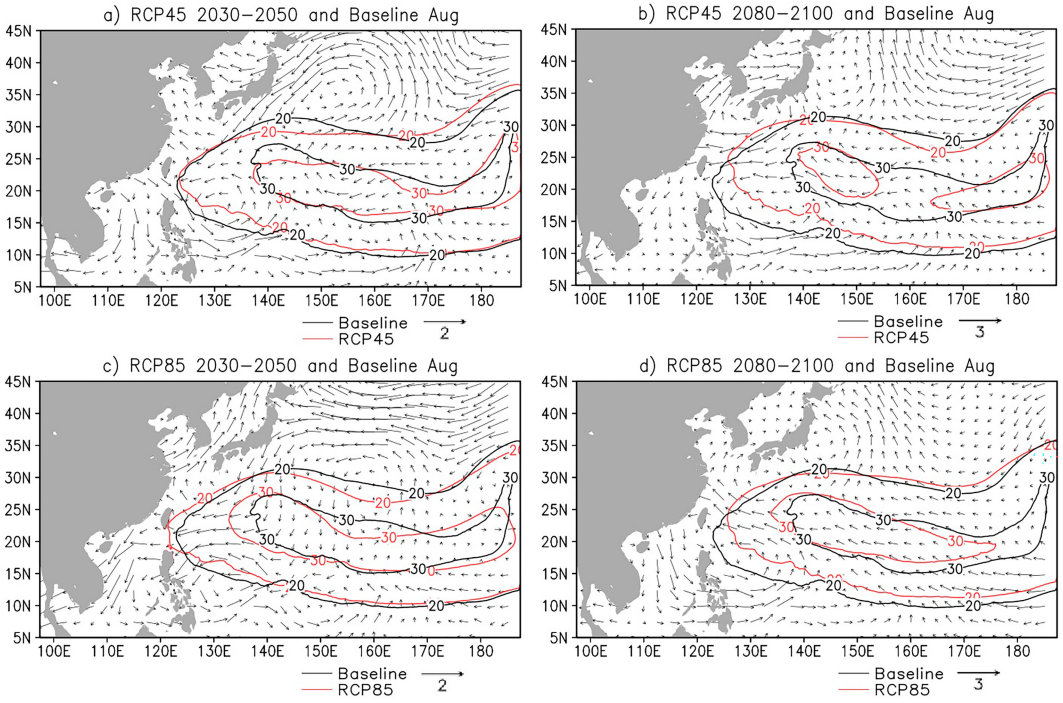

FIG. 13. As in Fig. 12, but for August.

or genesis distribution are also equally well captured by the same configuration. This is important for studying future changes in TC activities, because TC climatology must be then examined from several different angles.

Given the performance of our WRF configuration in recovering TC lifetime during the baseline period, a range of downscaling simulations for RCP4.5 and RCP8.5 were then carried out, with a focus on two future periods including the middle

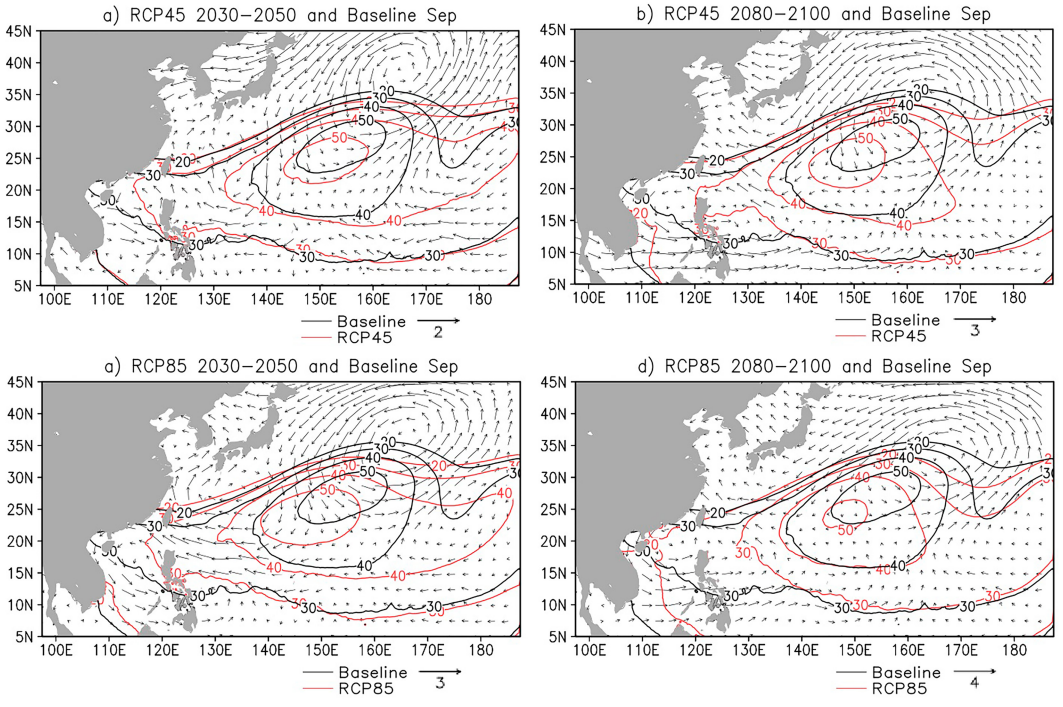

FIG. 14. As in Fig. 12, but for September.

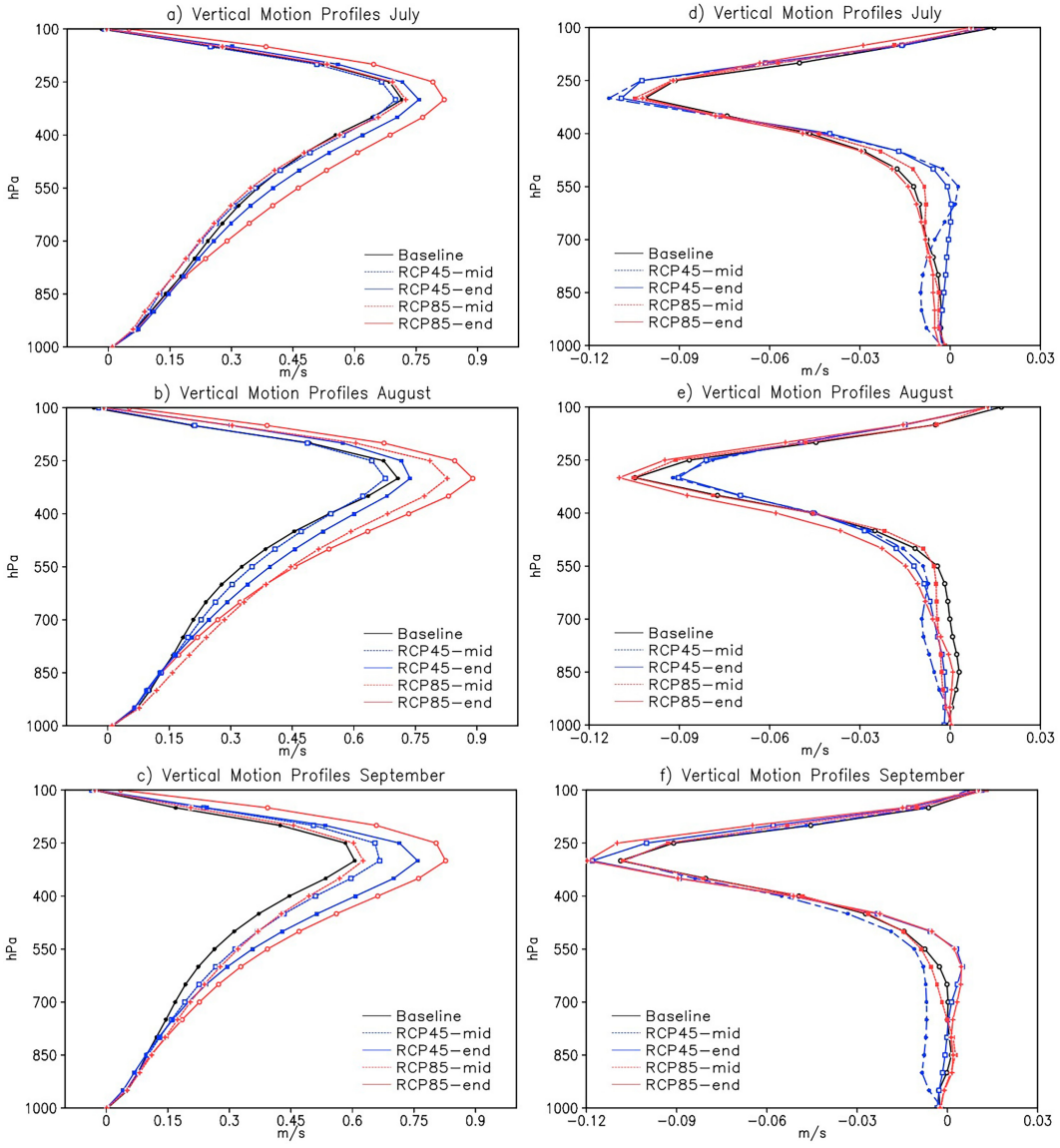

FIG. 15. Profiles of the mean vertical motion (m s^{-1}) averaged within (a)–(c) the ascending branch between 9° and 12°N and (d)–(f) the descending branch between 27° and 29°N of the Hadley circulation for the baseline and both future scenarios.

of the twenty-first century (2030–50) and the end of the twenty-first century (2080–2100). Comparison of TC statistics between the baseline and the four future periods captured several key results for TC climatology. First, we obtained a similar result as in previous studies that the lifetime maximum intensity in the WNP basin tends to increase across future scenarios, with a median changing from 40 in the baseline period to 45–47 m s^{-2}. For TC lifetime, future TCs do not, however, show any significant change in terms of the mean or median, regardless of the climate scenarios or future periods. This result is also consistent with previous studies, which captured inconclusive trends in the overall TC lifetime in the WNP basin.

Despite such insignificant changes in the TC lifetime mean and median, the TC lifetime distribution displayed a noticeable shift in the tails of the distribution, with more long-lived TCs (TC lifetime between 8 and 11 days). Likewise, there are fewer short-lived TCs in all future climates (i.e., TC lifetime between 3 and 5 days), albeit the change in the short-lived TCs is less significant as compared to long-lived TCs. The same increase in TC lifetime relative to the baseline period was also observed for the lower and upper percentiles of the TC lifetime distribution, but little difference among the future scenarios was found.

With those changes in TC lifetime distribution, we examined several potential mechanisms that can help understand

these changes, especially for the long-lived and the short-lived TCs. Following previous studies, we first explored the correlation between TC lifetime and Niño-3.4 index to see how the ENSO variability could be related to TC lifetime. While the Niño-3.4 index shows a positive correlation with TC lifetime during the baseline period as shown in previous studies, this relationship does not hold for future simulations in our future simulations. Specifically, the TC lifetime–Niño correlation becomes weaker for some future periods such as RCP4.5 2030–50, RCP4.5 2080–2100, and RCP8.5 2080–2100, and it even turned negative for RCP8.5 2030–50 period. This mixed correlation for different future periods suggests that the relationship between the TC lifetime and Niño-3.4 is less conclusive in the future, and so ENSO variability could not offer much insight into the change in TC lifetime as obtained herein.

To look for more direct causes of TC lifetime changes beyond the ENSO indices, TC track climatology was examined by grouping TC motion in the WNP basin into three main categories including straight-moving (SM), recurving landfall (RCL), and recurving ocean (RCO) TCs. Comparing the 20-yr averages between the baseline and the four future scenarios showed that the SM group has a minimum change, while both the RCL and RCO groups tend to shift more to the north in the future. In particular, the RCO group strongly veers to the open ocean rather than heading toward Japan's coastline under both future scenarios. This northeastward shift of TC tracks, along with insignificant changes in their translation speed, allows TCs to stay longer over the open ocean, thus generating more long-lived TCs as seen in our downscaling.

Because TC track patterns are governed by large-scale steering flows, any change in TC track patterns should be related to the variability of large-scale circulations. To understand the specific change in the RCO track group, we thus analyzed the western Pacific subtropical high (WPSH) for different future periods. Using the geopotential height anomalies at 500 hPa as a proxy for WPSH, we found that WPSH tends to be pushed gradually to the south during July and shifted to the northeast during August–September in all future scenarios. In addition, the future WPSH is stronger as compared to the baseline period, especially toward the end of the twenty-first century. As a result of these shifting and strengthening of the WPSH, the easterly steering flows on WPSH's southern flank are reduced in the future, thus less likely to steer TCs toward the coastal areas as in the baseline period. The stronger WPSH obtained in our future downscaling also accords with the strengthening of the Hadley circulation across future periods and scenarios.

Given our WRF Model configuration and the downscaling settings in this study, a number of caveats should be mentioned. First, our downscaling simulations were conducted with a single model and the CESM global input, with no sensitivity analyses for different model configurations or other input data. Such a limitation is due to the heavy computational resources and storage associated with homogeneous high-resolution settings and model output for tracking TCs in this study. The lack of such sensitivity may affect the robustness of our findings, especially for future projections for which there is no observation to cross validate. Despite this lack of model sensitivity analyses, we wish to note that our results are still of significance in the sense that we focus more on the epochal average for 20-yr periods rather than a single-year event. As such, the statistics are expected to capture the key signal, albeit there are potentially some model biases that we could not fully eliminate.

Second, more in-depth analyses of extreme statistics are still needed to account for other climate factors such as quasi-biennial oscillation (QBO) or Pacific decadal oscillation, which may also affect TC lifetime statistics beyond 20-yr windows. In our analyses, we note that a 20-yr average was applied as a means to measure epochal changes in TC climatology, but these 20-yr periods may still contain some decadal modes that could interfere with our analyses. Regardless of the contribution from these decadal modes, the physical causes for any changes in TC lifetime must be linked eventually to the overall TC track patterns and large-scale circulations in the WNP basin. From this perspective, our analyses could provide some clues about the mechanisms underlying TC lifetime changes, even in the presence of other internal decadal modes. Future work using a longer downscaling period or climate model averages from other future scenarios can help validate our findings here further, which are still highly uncertain due to different mechanisms and offsets.

Acknowledgments. This research was partially supported by ONR Award (N000142012411) and NSF Grant AGS-2309929. Support for BK was provided in part by the Indiana University Environmental Resilience Institute. The Pacific Northwest National Laboratory is operated for the U.S. Department of Energy by Battelle Memorial Institute under Contract DE-AC05-76RL01830. PWS was supported by NSF Grant 2140235. We also wish to thank three anonymous reviewers for their constructive comments that have helped improve this work substantially and Hue Nguyen for her assistance in some of the analyses. The IU Research Support System for providing the high-performance computing resource for this study is greatly acknowledged, which was supported in part by Lilly Endowment, Inc., through its support for the Indiana University Pervasive Technology Institute.

Data availability statement. The CESM bias-corrected projection dataset used in this study is available at https://rda.ucar.edu/datasets/ds316.1/, and the best track TC data are available at https://www.ncei.noaa.gov/products/international-best-track-archive.

REFERENCES

Bengtsson, L., K. I. Hodges, M. Esch, N. Keenlyside, L. Kornblueh, J.-J. Luo, and T. Yamagata, 2007: How may tropical cyclones change in a warmer climate? *Tellus*, **59A**, 539–561, https://doi.org/10.1111/j.1600-0870.2007.00251.x.

Bruyère, C. L., J. M. Done, G. J. Holland, and S. Fredrick, 2014: Bias corrections of global models for regional climate

simulations of high-impact weather. *Climate Dyn.*, **43**, 1847–1856, https://doi.org/10.1007/s00382-013-2011-6.

Cai, W., and Coauthors, 2021: Changing El Niño–Southern Oscillation in a warming climate. *Nat. Rev. Earth Environ.*, **2**, 628–644, https://doi.org/10.1038/s43017-021-00199-z.

Camargo, S. J., 2013: Global and regional aspects of tropical cyclone activity in the CMIP5 models. *J. Climate*, **26**, 9880–9902, https://doi.org/10.1175/JCLI-D-12-00549.1.

——, and A. H. Sobel, 2005: Western North Pacific tropical cyclone intensity and ENSO. *J. Climate*, **18**, 2996–3006, https://doi.org/10.1175/JCLI3457.1.

——, K. A. Emanuel, and A. H. Sobel, 2007a: Use of a genesis potential index to diagnose ENSO effects on tropical cyclone genesis. *J. Climate*, **20**, 4819–4834, https://doi.org/10.1175/JCLI4282.1.

——, A. W. Robertson, S. J. Gaffney, P. Smyth, and M. Ghil, 2007b: Cluster analysis of typhoon tracks. Part I: General properties. *J. Climate*, **20**, 3635–3653, https://doi.org/10.1175/JCLI4188.1.

——, and Coauthors, 2023: An update on the influence of natural climate variability and anthropogenic climate change on tropical cyclones. *Trop. Cyclone Res. Rev.*, **12**, 216–239, https://doi.org/10.1016/j.tcrr.2023.10.001.

Cha, E. J., T. R. Knutson, T.-C. Lee, M. Ying, and T. Nakaegawa, 2020: Third assessment on impacts of climate change on tropical cyclones in the typhoon committee region—Part II: Future projections. *Trop. Cyclone Res. Rev.*, **9**, 75–86, https://doi.org/10.1016/j.tcrr.2020.04.005.

Chan, J. C. L., 2000: Tropical cyclone activity over the western North Pacific associated with El Niño and La Niña events. *J. Climate*, **13**, 2960–2972, https://doi.org/10.1175/1520-0442(2000)013%3C2960:TCAOTW%3E2.0.CO;2.

——, 2008: Decadal variations of intense typhoon occurrence in the western North Pacific. *Proc. Roy. Soc.*, **464A**, 249–272, https://doi.org/10.1098/rspa.2007.0183.

——, and K. S. Liu, 2004: Global warming and western North Pacific typhoon activity from an observational perspective. *J. Climate*, **17**, 4590–4602, https://doi.org/10.1175/3240.1.

Christensen, J. H., F. Boberg, O. B. Christensen, and P. Lucas-Picher, 2008: On the need for bias correction of regional climate change projections of temperature and precipitation. *Geophys. Res. Lett.*, **35**, L20709, https://doi.org/10.1029/2008GL035694.

Chung, P.-H., C.-H. Sui, and T. Li, 2011: Interannual relationships between the tropical sea surface temperature and summertime subtropical anticyclone over the western North Pacific. *J. Geophys. Res.*, **116**, D13111, https://doi.org/10.1029/2010JD015554.

Colbert, A. J., B. J. Soden, G. A. Vecchi, and B. P. Kirtman, 2013: The impact of anthropogenic climate change on North Atlantic tropical cyclone tracks. *J. Climate*, **26**, 4088–4095, https://doi.org/10.1175/JCLI-D-12-00342.1.

——, ——, and B. P. Kirtman, 2015: The impact of natural and anthropogenic climate change on western North Pacific tropical cyclone tracks. *J. Climate*, **28**, 1806–1823, https://doi.org/10.1175/JCLI-D-14-00100.1.

Dao, L. T., and J.-Y. Yu, 2022: Changes of local tropical cyclone activity over the South China Sea under global warming in high-resolution atmospheric model projections. *Int. J. Climatol.*, **42**, 2965–2980, https://doi.org/10.1002/joc.7401.

Davis, C. A., 2018: Resolving tropical cyclone intensity in models. *Geophys. Res. Lett.*, **45**, 2082–2087, https://doi.org/10.1002/2017GL076966.

Defforge, C. L., and T. M. Merlis, 2017: Observed warming trend in sea surface temperature at tropical cyclone genesis. *Geophys. Res. Lett.*, **44**, 1034–1040, https://doi.org/10.1002/2016GL071045.

Denis, B., R. Laprise, D. Caya, and J. Côté, 2002: Downscaling ability of one-way nested regional climate models: The big-brother experiment. *Climate Dyn.*, **18**, 627–646, https://doi.org/10.1007/s00382-001-0201-0.

Emanuel, K. A., 1987: The dependence of hurricane intensity on climate. *Nature*, **326**, 483–485, https://doi.org/10.1038/326483a0.

Gastineau, G., L. Li, and H. L. Treut, 2009: The Hadley and Walker circulation changes in global warming conditions described by idealized atmospheric simulations. *J. Climate*, **22**, 3993–4013, https://doi.org/10.1175/2009JCLI2794.1.

Giorgi, F., and L. O. Mearns, 1999: Introduction to special section: Regional climate modeling revisited. *J. Geophys. Res.*, **104**, 6335–6352, https://doi.org/10.1029/98JD02072.

Harr, P. A., and R. L. Elsberry, 1991: Tropical cyclone track characteristics as a function of large-scale circulation anomalies. *Mon. Wea. Rev.*, **119**, 1448–1468, https://doi.org/10.1175/1520-0493(1991)119%3C1448:TCTCAA%3E2.0.CO;2.

He, C., and T. Zhou, 2015: Responses of the western North Pacific subtropical high to global warming under RCP4.5 and RCP8.5 scenarios projected by 33 CMIP5 models: The dominance of tropical Indian Ocean–tropical western Pacific SST gradient. *J. Climate*, **28**, 365–380, https://doi.org/10.1175/JCLI-D-13-00494.1.

Hill, K. A., and G. M. Lackmann, 2011: The impact of future climate change on TC intensity and structure: A downscaling approach. *J. Climate*, **24**, 4644–4661, https://doi.org/10.1175/2011JCLI3761.1.

Ho, C.-H., J.-J. Baik, J.-H. Kim, D.-Y. Gong, and C.-H. Sui, 2004: Interdecadal changes in summertime typhoon tracks. *J. Climate*, **17**, 1767–1776, https://doi.org/10.1175/1520-0442(2004)017<1767:ICISTT>2.0.CO;2.

Holland, G. J., 1997: The maximum potential intensity of tropical cyclones. *J. Atmos. Sci.*, **54**, 2519–2541, https://doi.org/10.1175/1520-0469(1997)054<2519:TMPIOT>2.0.CO;2.

Hong, C.-C., C.-H. Tsou, P.-C. Hsu, K.-C. Chen, H.-C. Liang, H.-H. Hsu, C.-Y. Tu, and A. Kitoh, 2021: Future changes in tropical cyclone intensity and frequency over the western North Pacific based on 20-km HiRAM and MRI models. *J. Climate*, **34**, 2235–2251, https://doi.org/10.1175/JCLI-D-20-0417.1.

Huang, X., T. Zhou, J. C. L. Chan, R. Zhan, Z. Chen, and J. Zhao, 2023: Understanding uncertainties in projections of western North Pacific tropical cyclogenesis. *Environ. Res. Lett.*, **18**, 114037, https://doi.org/10.1088/1748-9326/ad02ad.

Hurrell, J. W., and Coauthors, 2013: The Community Earth System Model: A framework for collaborative research. *Bull. Amer. Meteor. Soc.*, **94**, 1339–1360, https://doi.org/10.1175/BAMS-D-12-00121.1.

Jin, C.-S., C.-H. Ho, J.-H. Kim, D.-K. Lee, D.-H. Cha, and S.-W. Yeh, 2013: Critical role of northern off-equatorial sea surface temperature forcing associated with central Pacific El Niño in more frequent tropical cyclone movements toward East Asia. *J. Climate*, **26**, 2534–2545, https://doi.org/10.1175/JCLI-D-12-00287.1.

——, D.-H. Cha, D.-K. Lee, M.-S. Suh, S.-Y. Hong, H.-S. Kang, and C.-H. Ho, 2016: Evaluation of climatological tropical cyclone activity over the western North Pacific in the CORDEX-East Asia multi-RCM simulations. *Climate Dyn.*, **47**, 765–778, https://doi.org/10.1007/s00382-015-2869-6.

Jourdain, N. C., P. Marchesiello, C. E. Menkes, J. Lefèvre, E. M. Vincent, M. Lengaigne, and F. Chauvin, 2011: Mesoscale simulation of tropical cyclones in the South Pacific: Climatology and interannual variability. *J. Climate*, **24**, 3–25, https://doi.org/10.1175/2010JCLI3559.1.

Jullien, S., P. Marchesiello, C. E. Menkes, J. Lefèvre, N. C. Jourdain, G. Samson, and M. Lengaigne, 2014: Ocean feedback to tropical cyclones: Climatology and processes. *Climate Dyn.*, **43**, 2831–2854, https://doi.org/10.1007/s00382-014-2096-6.

Kain, J. S., and J. M. Fritsch, 1990: A one-dimensional entraining/detraining plume model and its application in convective parameterization. *J. Atmos. Sci.*, **47**, 2784–2802, https://doi.org/10.1175/1520-0469(1990)047<2784:AODEPM>2.0.CO;2.

Kieu, C., M. Zhao, Z. Tan, B. Zhang, and T. Knutson, 2023: On the role of sea surface temperature in the clustering of global tropical cyclone formation. *J. Climate*, **36**, 3145–3162, https://doi.org/10.1175/JCLI-D-22-0623.1.

Kim, D., C.-S. Jin, C.-H. Ho, J. Kim, and J.-H. Kim, 2015: Climatological features of WRF-simulated tropical cyclones over the western North Pacific. *Climate Dyn.*, **44**, 3223–3235, https://doi.org/10.1007/s00382-014-2410-3.

Kim, H.-M., M.-I. Lee, P. J. Webster, D. Kim, and J. H. Yoo, 2013: A physical basis for the probabilistic prediction of the accumulated tropical cyclone kinetic energy in the western North Pacific. *J. Climate*, **26**, 7981–7991, https://doi.org/10.1175/JCLI-D-12-00679.1.

Kim, H.-S., G. A. Vecchi, T. R. Knutson, W. G. Anderson, T. L. Delworth, A. Rosati, F. Zeng, and M. Zhao, 2014: Tropical cyclone simulation and response to CO_2 doubling in the GFDL CM2.5 high-resolution coupled climate model. *J. Climate*, **27**, 8034–8054, https://doi.org/10.1175/JCLI-D-13-00475.1.

Kirtman, B. P., 2014: The North American Multimodel Ensemble: Phase-1 seasonal-to-interannual prediction; phase-2 toward developing intraseasonal prediction. *Bull. Amer. Meteor. Soc.*, **95**, 585–601, https://doi.org/10.1175/BAMS-D-12-00050.1.

Knutson, T. R., R. E. Tuleya, and Y. Kurihara, 1998: Simulated increase of hurricane intensities in a CO_2-warmed climate. *Science*, **279**, 1018–1021, https://doi.org/10.1126/science.279.5353.1018.

——, J. J. Sirutis, S. T. Garner, I. M. Held, and R. E. Tuleya, 2007: Simulation of the recent multidecadal increase of Atlantic hurricane activity using an 18-km-grid regional model. *Bull. Amer. Meteor. Soc.*, **88**, 1549–1565, https://doi.org/10.1175/BAMS-88-10-1549.

——, ——, ——, G. A. Vecchi, and I. M. Held, 2008: Simulated reduction in Atlantic hurricane frequency under twenty-first-century warming conditions. *Nat. Geosci.*, **1**, 359–364, https://doi.org/10.1038/ngeo202.

——, and Coauthors, 2010: Tropical cyclones and climate change. *Nat. Geosci.*, **3**, 157–163, https://doi.org/10.1038/ngeo779.

Kossin, J. P., K. A. Emanuel, and S. J. Camargo, 2016: Past and projected changes in western North Pacific tropical cyclone exposure. *J. Climate*, **29**, 5725–5739, https://doi.org/10.1175/JCLI-D-16-0076.1.

Kotlarski, S., S. Hagemann, P. Krahe, R. Podzun, and D. Jacob, 2012: The Elbe river flooding 2002 as seen by an extended regional climate model. *J. Hydrol.*, **472–473**, 169–183, https://doi.org/10.1016/j.jhydrol.2012.09.020.

Lee, C.-Y., S. J. Camargo, F. Vitart, A. H. Sobel, J. Camp, S. Wang, M. K. Tippett, and Q. Yang, 2020: Subseasonal predictions of tropical cyclone occurrence and ace in the S2S dataset. *Wea. Forecasting*, **35**, 921–938, https://doi.org/10.1175/WAF-D-19-0217.1.

Lee, H., C.-S. Jin, D.-H. Cha, M. Lee, D.-K. Lee, M.-S. Suh, S.-Y. Hong, and H.-S. Kang, 2019: Future change in tropical cyclone activity over the western North Pacific in CORDEX-East Asia multi-RCMs forced by HadGEM2-AO. *J. Climate*, **32**, 5053–5067, https://doi.org/10.1175/JCLI-D-18-0575.1.

Lee, T.-C., T. R. Knutson, T. Nakaegawa, M. Ying, and E. J. Cha, 2020: Third assessment on impacts of climate change on tropical cyclones in the typhoon committee region—Part I: Observed changes, detection and attribution. *Trop. Cyclone Res. Rev.*, **9** (1), 1–22, https://doi.org/10.1016/j.tcrr.2020.03.001.

Lin, Y.-L., R. D. Farley, and H. D. Orville, 1983: Bulk parameterization of the snow field in a cloud model. *J. Climate Appl. Meteor.*, **22**, 1065–1092, https://doi.org/10.1175/1520-0450(1983)022%3C1065:BPOTSF%3E2.0.CO;2.

Liu, M., G. A. Vecchi, J. A. Smith, and T. R. Knutson, 2019: Causes of large projected increases in hurricane precipitation rates with global warming. *npj Climate Atmos. Sci.*, **2**, 38, https://doi.org/10.1038/s41612-019-0095-3.

Liu, Y., W. Li, J. Zuo, and Z.-Z. Hu, 2014: Simulation and projection of the western Pacific subtropical high in CMIP5 models. *J. Meteor. Res.*, **28**, 327–340, https://doi.org/10.1007/s13351-014-3151-2.

Lu, J., G. A. Vecchi, and T. Reichler, 2007: Expansion of the Hadley cell under global warming. *Geophys. Res. Lett.*, **34**, L06805, https://doi.org/10.1029/2006GL028443.

Lucas-Picher, P., F. Boberg, J. H. Christensen, and P. Berg, 2013: Dynamical downscaling with reinitializations: A method to generate finescale climate datasets suitable for impact studies. *J. Hydrometeor.*, **14**, 1159–1174, https://doi.org/10.1175/JHM-D-12-063.1.

Manganello, J. V., and Coauthors, 2014: Future changes in the western North Pacific tropical cyclone activity projected by a multidecadal simulation with a 16-km global atmospheric GCM. *J. Climate*, **27**, 7622–7646, https://doi.org/10.1175/JCLI-D-13-00678.1.

McDonald, R. E., D. G. Bleaken, D. R. Cresswell, V. D. Pope, and C. A. Senior, 2005: Tropical storms: Representation and diagnosis in climate models and the impacts of climate change. *Climate Dyn.*, **25**, 19–36, https://doi.org/10.1007/s00382-004-0491-0.

Mlawer, E. J., S. J. Taubman, P. D. Brown, M. J. Iacono, and S. A. Clough, 1997: Radiative transfer for inhomogeneous atmospheres: RRTM, a validated correlated-k model for the longwave. *J. Geophys. Res.*, **102**, 16 663–16 682, https://doi.org/10.1029/97JD00237.

Murakami, H., and M. Sugi, 2010: Effect of model resolution on tropical cyclone climate projections. *SOLA*, **6**, 73–76, https://doi.org/10.2151/sola.2010-019.

——, B. Wang, and A. Kitoh, 2011: Future change of western North Pacific typhoons: Projections by a 20-km-mesh global atmospheric model. *J. Climate*, **24**, 1154–1169, https://doi.org/10.1175/2010JCLI3723.1.

——, P.-C. Hsu, O. Arakawa, and T. Li, 2014: Influence of model biases on projected future changes in tropical cyclone frequency of occurrence. *J. Climate*, **27**, 2159–2181, https://doi.org/10.1175/JCLI-D-13-00436.1.

Oouchi, K., J. Yoshimura, H. Yoshimura, R. Mizuta, S. Kusunoki, and A. Noda, 2006: Tropical cyclone climatology in a global-warming climate as simulated in a 20 km-mesh global atmospheric model: Frequency and wind intensity analyses. *J. Meteor. Soc. Japan*, **84**, 259–276, https://doi.org/10.2151/jmsj.84.259.

Peduzzi, P., B. Chatenoux, H. Dao, A. D. Bono, C. Herold, J. Kossin, F. Mouton, and O. Nordbeck, 2012: Global trends

in tropical cyclone risk. *Nat. Climate Change*, **2**, 289–294, https://doi.org/10.1038/nclimate1410.

Qian, J.-H., A. Seth, and S. Zebiak, 2003: Reinitialized versus continuous simulations for regional climate downscaling. *Mon. Wea. Rev.*, **131**, 2857–2874, https://doi.org/10.1175/1520-0493(2003)131%3C2857:RVCSFR%3E2.0.CO;2.

Redmond, G., K. I. Hodges, C. Mcsweeney, R. Jones, and D. Hein, 2015: Projected changes in tropical cyclones over Vietnam and the South China Sea using a 25 km regional climate model perturbed physics ensemble. *Climate Dyn.*, **45**, 1983–2000, https://doi.org/10.1007/s00382-014-2450-8.

Richter, J. H., and Coauthors, 2020: Subseasonal prediction with and without a well-represented stratosphere in CESM1. *Wea. Forecasting*, **35**, 2589–2602, https://doi.org/10.1175/WAF-D-20-0029.1.

Royer, J.-F., F. Chauvin, B. Timbal, P. Araspin, and D. Grimal, 1998: A GCM study of the impact of greenhouse gas increase on the frequency of occurrence of tropical cyclones. *Climatic Change*, **38**, 307–343, https://doi.org/10.1023/A:1005386312622.

Skamarock, W. C., and Coauthors, 2008: A description of the Advanced Research WRF version 3. NCAR Tech. Note NCAR/TN-475+STR, 113 pp., https://doi.org/10.5065/D68S4MVH.

Su, H., J. H. Jiang, C. Zhai, T. J. Shen, J. D. Neelin, G. L. Stephens, and Y. L. Yung, 2014: Weakening and strengthening structures in the Hadley Circulation change under global warming and implications for cloud response and climate sensitivity. *J. Geophys. Res. Atmos.*, **119**, 5787–5805, https://doi.org/10.1002/2014JD021642.

Sugi, M., A. Noda, and N. Sato, 2002: Influence of the global warming on tropical cyclone climatology: An experiment with the JMA global model. *J. Meteor. Soc. Japan*, **80**, 249–272, https://doi.org/10.2151/jmsj.80.249.

Tang, Y., J. Huangfu, R. Huang, and W. Chen, 2022: Simulation and projection of tropical cyclone activities over the western North Pacific by CMIP6 HighResMIP. *J. Climate*, **35**, 7771–7794, https://doi.org/10.1175/JCLI-D-21-0760.1.

Tao, S. Y., and L. X. Chen, 1987: A review of recent research on the East Asian summer monsoon in China. *Monsoon Meteor.*, C.-P. Chang and T.N. Krishnamurti, Eds., Oxford University Press, 60–92.

Taylor, K. E., R. J. Stouffer, and G. A. Meehl, 2012: An overview of CMIP5 and the experiment design. *Bull. Amer. Meteor. Soc.*, **93**, 485–498, https://doi.org/10.1175/BAMS-D-11-00094.1.

Thanh, N. T., H. D. Cuong, N. X. Hien, and C. Kieu, 2020: Relationship between sea surface temperature and the maximum intensity of tropical cyclones affecting Vietnam's coastline. *Int. J. Climatol.*, **40**, 2527–2538, https://doi.org/10.1002/joc.6348.

Tran-Quang, D., H. Pham-Thanh, T.-A. Vu, C. Kieu, and T. Phan-Van, 2020: Climatic shift of the tropical cyclone activity affecting Vietnam's coastal region. *J. Appl. Meteor. Climatol.*, **59**, 1755–1768, https://doi.org/10.1175/JAMC-D-20-0021.1.

Trinh, D. H., H. D. Cuong, D. V. Kham, and C. Kieu, 2021: Remote control of sea surface temperature on the variability of tropical cyclone activity affecting Vietnam's coastline. *J. Appl. Meteor. Climatol.*, **60**, 323–339, https://doi.org/10.1175/JAMC-D-20-0170.1.

Tsou, C. H., P.-Y. Huang, C.-Y. Tu, C.-T. Chen, T.-P. Tzeng, and C.-T. Cheng, 2016: Present simulation and future typhoon activity projection over western North Pacific and Taiwan/East Coast of China in 20-km HiRAM climate model. *Terr. Atmos. Ocean. Sci.*, **27**, 687–703, https://doi.org/10.3319/TAO.2016.06.13.04.

Tulich, S. N., G. N. Kiladis, and A. Suzuki-Parker, 2011: Convectively coupled Kelvin and easterly waves in a regional climate simulation of the tropics. *Climate Dyn.*, **36**, 185–203, https://doi.org/10.1007/s00382-009-0697-2.

Vecchi, G. A., and B. J. Soden, 2007: Global warming and the weakening of the tropical circulation. *J. Climate*, **20**, 4316–4340, https://doi.org/10.1175/JCLI4258.1.

——, and Coauthors, 2019: Tropical cyclone sensitivities to CO_2 doubling: Roles of atmospheric resolution, synoptic variability and background climate changes. *Climate Dyn.*, **53**, 5999–6033, https://doi.org/10.1007/s00382-019-04913-y.

Vu, T.-A., C. Kieu, D. Chavas, and Q. Wang, 2021: A numerical study of the global formation of tropical cyclones. *J. Adv. Model. Earth Syst.*, **13**, e2020MS002207, https://doi.org/10.1029/2020MS002207.

Walsh, K. J. E., and B. F. Ryan, 2000: Tropical cyclone intensity increase near Australia as a result of climate change. *J. Climate*, **13**, 3029–3036, https://doi.org/10.1175/1520-0442(2000)013%3C3029:TCIINA%3E2.0.CO;2.

——, M. Fiorino, C. W. Landsea, and K. L. McInnes, 2007: Objectively determined resolution-dependent threshold criteria for the detection of tropical cyclones in climate models and reanalyses. *J. Climate*, **20**, 2307–2314, https://doi.org/10.1175/JCLI4074.1.

Wang, B., and J. C. L. Chan, 2002: How strong ENSO events affect tropical storm activity over the western North Pacific. *J. Climate*, **15**, 1643–1658, https://doi.org/10.1175/1520-0442(2002)015<1643:HSEEAT>2.0.CO;2.

Warner, T. T., R. A. Peterson, and R. E. Treadon, 1997: A tutorial on lateral boundary conditions as a basic and potentially serious limitation to regional numerical weather prediction. *Bull. Amer. Meteor. Soc.*, **78**, 2599–2618, https://doi.org/10.1175/1520-0477(1997)078%3C2599:ATOLBC%3E2.0.CO;2.

Wu, B., and T. Zhou, 2008: Oceanic origin of the interannual and interdecadal variability of the summertime western Pacific Subtropical High. *Geophys. Res. Lett.*, **35**, L13701, https://doi.org/10.1029/2008GL034584.

Wu, L., and B. Wang, 2004: Assessing impacts of global warming on tropical cyclone tracks. *J. Climate*, **17**, 1686–1698, https://doi.org/10.1175/1520-0442(2004)017<1686:AIOGWO>2.0.CO;2.

——, and H. Zhao, 2012: Dynamically derived tropical cyclone intensity changes over the western North Pacific. *J. Climate*, **25**, 89–98, https://doi.org/10.1175/2011JCLI4139.1.

——, B. Wang, and S. Geng, 2005: Growing typhoon influence on East Asia. *Geophys. Res. Lett.*, **32**, L18703, https://doi.org/10.1029/2005GL022937.

Yeager, S. G., and Coauthors, 2018: Predicting near-term changes in the Earth system: A large ensemble of initialized decadal prediction simulations using the Community Earth System Model. *Bull. Amer. Meteor. Soc.*, **99**, 1867–1886, https://doi.org/10.1175/BAMS-D-17-0098.1.

Yihui, D., and J. C. L. Chan, 2005: The East Asian summer monsoon: An overview. *Meteor. Atmos. Phys.*, **89**, 117–142, https://doi.org/10.1007/s00703-005-0125-z.

Yokoi, S., C. Takahashi, K. Yasunaga, and R. Shirooka, 2012: Multi-model projection of tropical cyclone genesis frequency over the Western North Pacific: CMIP5 results. *SOLA*, **8**, 137–140, https://doi.org/10.2151/sola.2012-034.

——, Y. N. Takayabu, and H. Murakami, 2013: Attribution of projected future changes in tropical cyclone passage frequency over the western North Pacific. *J. Climate*, **26**, 4096–4111, https://doi.org/10.1175/JCLI-D-12-00218.1.

Yonekura, E., and T. M. Hall, 2011: A statistical model of tropical cyclone tracks in the western North Pacific with ENSO-dependent cyclogenesis. *J. Appl. Meteor. Climatol.*, **50**, 1725–1739, https://doi.org/10.1175/2011JAMC2617.1.

Yoshimura, J., M. Sugi, and A. Noda, 2006: Influence of greenhouse warming on tropical cyclone frequency. *J. Meteor. Soc. Japan*, **84**, 405–428, https://doi.org/10.2151/jmsj.84.405.

Zhang, C., and Y. Wang, 2017: Projected future changes of tropical cyclone activity over the western North and South Pacific in a 20-km-mesh regional climate model. *J. Climate*, **30**, 5923–5941, https://doi.org/10.1175/JCLI-D-16-0597.1.

Zhang, L., and T. L. Delworth, 2016: Simulated response of the Pacific decadal oscillation to climate change. *J. Climate*, **29**, 5999–6018, https://doi.org/10.1175/JCLI-D-15-0690.1.

Zhao, H., and L. Wu, 2014: Inter-decadal shift of the prevailing tropical cyclone tracks over the western North Pacific and its mechanism study. *Meteor. Atmos. Phys.*, **125**, 89–101, https://doi.org/10.1007/s00703-014-0322-8.

——, ——, and W. Zhou, 2010: Assessing the influence of the ENSO on tropical cyclone prevailing tracks in the western North Pacific. *Adv. Atmos. Sci.*, **27**, 1361–1371, https://doi.org/10.1007/s00376-010-9161-9.

Zhao, M., I. M. Held, S.-J. Lin, and G. A. Vecchi, 2009: Simulations of global hurricane climatology, interannual variability, and response to global warming using a 50-km resolution GCM. *J. Climate*, **22**, 6653–6678, https://doi.org/10.1175/2009JCLI3049.1.